

Heat Transfer Tests of Ribbed Surfaces for Gas-Cooled Reactors

O. H. Klepper



OAK RIDGE NATIONAL LABORATORY

OPERATED BY UNION CARBIDE CORPORATION • FOR THE U.S. ATOMIC ENERGY COMMISSION

MASTER

DISTRIBUTION OF THIS DOCUMENT UNLIMITED

DISCLAIMER

This report was prepared as an account of work sponsored by an agency of the United States Government. Neither the United States Government nor any agency Thereof, nor any of their employees, makes any warranty, express or implied, or assumes any legal liability or responsibility for the accuracy, completeness, or usefulness of any information, apparatus, product, or process disclosed, or represents that its use would not infringe privately owned rights. Reference herein to any specific commercial product, process, or service by trade name, trademark, manufacturer, or otherwise does not necessarily constitute or imply its endorsement, recommendation, or favoring by the United States Government or any agency thereof. The views and opinions of authors expressed herein do not necessarily state or reflect those of the United States Government or any agency thereof.

DISCLAIMER

Portions of this document may be illegible in electronic image products. Images are produced from the best available original document.

Printed in the United States of America. Available from
National Technical Information Service
U.S. Department of Commerce
5285 Port Royal Road, Springfield, Virginia 22161
Price: Printed Copy \$5.45; Microfiche \$2.25

This report was prepared as an account of work sponsored by the United States Government. Neither the United States nor the Energy Research and Development Administration, nor any of their employees, nor any of their contractors, subcontractors, or their employees, makes any warranty, express or implied, or assumes any legal liability or responsibility for the accuracy, completeness or usefulness of any information, apparatus, product or process disclosed, or represents that its use would not infringe privately owned rights.

ORNL-TM-4108
UC-77 - Gas Cooled
Reactor Technology

Contract No. W-7405-eng-26

Reactor Division

NOTICE
This report was prepared as an account of work sponsored by the United States Government. Neither the United States nor the United States Energy Research and Development Administration, nor any of their employees, nor any of their contractors, subcontractors, or their employees, makes any warranty, express or implied, or assumes any legal liability or responsibility for the accuracy, completeness or usefulness of any information, apparatus, product or process disclosed, or represents that its use would not infringe privately owned rights.

HEAT TRANSFER TESTS OF RIBBED SURFACES
FOR GAS-COOLED REACTORS

O. H. Klepper

JULY 1975

OAK RIDGE NATIONAL LABORATORY
Oak Ridge, Tennessee 37830
Operated by
UNION CARBIDE CORPORATION
for the
U.S. ENERGY RESEARCH AND DEVELOPMENT ADMINISTRATION

MASTER

DISTRIBUTION OF THIS DOCUMENT UNLIMITED

THIS PAGE
WAS INTENTIONALLY
LEFT BLANK

CONTENTS

	<u>Page</u>
Acknowledgement	v
ABSTRACT	1
1. INTRODUCTION	1
2. EXPERIMENTAL EQUIPMENT AND PROCEDURES	2
2.1 Test Facility	2
2.2 Heater Rods	8
2.3 Test Conditions	10
3. DATA REDUCTION AND TRANSFORMATIONS	13
3.1 Heat Transfer Calculations	14
3.2 Friction Factor Calculations	14
3.3 Transformations	16
3.3.1 Friction Factor Transformation	18
3.3.2 Stanton Modulus Transformation	21
4. RESULTS AND DISCUSSION	22
4.1 Pressure Drop Results	22
4.2 Heat Transfer Results	26
4.3 Comparison with Other Results	31
5. SURFACE EFFECTIVENESS	35
6. CONCLUSIONS	37
REFERENCES	38
LIST OF SYMBOLS	40
Appendix A	43

THIS PAGE
WAS INTENTIONALLY
LEFT BLANK

ACKNOWLEDGEMENTS

This research, performed at the Oak Ridge National Laboratory, was sponsored by the U. S. Atomic Energy Commission under contract with Union Carbide Corporation.

The author is grateful for the assistance given by R. H. Jones in the design of the test section and for that by J. W. Krewson in the development of the test loop and the associated instrumentation. D. L. Clark's help in the design and procurement of the heater rods, as well as General Atomics Company's cooperation in the preparation of the test surfaces, is gratefully acknowledged. G. Markóczy was most helpful by providing comparative test results obtained at the Eidg. Institut für Reaktorforschung in Würenlinge, Switzerland, and by suggesting some useful methods for data analysis.

For the preparation of the report I thank Margie Adair and Viola Erickson.

HEAT TRANSFER TESTS OF RIBBED SURFACES FOR GAS-COOLED REACTORS

O. H. Klepper

ABSTRACT

The performance of gas-cooled reactors is often limited by the heat transfer in the reactor core. The present studies have investigated means for modifying core heat transfer surfaces to improve their performance. Experiments were conducted to evaluate several rod surfaces roughened by GA for ORNL. The 0.3-in.-OD stainless steel clad heater rods were photo-etched to produce external ribs 0.006 in. high and 0.12 in. wide with a pitch of 0.072 in. Helical ribs with a helix angle of 37 deg (to promote interchannel flow mixing in a multirod array) were provided on one surface. For comparison purposes, a transversely ribbed surface and a smooth rod were also studied. The test surfaces were 49 in. long with a 24-in. heated region, concentrically arranged inside a smooth 0.602-in.-ID stainless steel tube. Nitrogen gas at pressures up to 400 psig was used as the coolant; the linear heat rating ranged to 6.8 kW/ft at surface temperatures up to 1400°F; T_w/T_b varied from 1.2 to 2.4 at Re values up to 450,000. Annulus results were recalculated for rod geometry using two different transformations. Good agreement was observed with applicable literature values.

The effectiveness of the surfaces was assessed as the ratio E of the heat transfer coefficients of the roughened rods to that of a smooth rod at the same pumping power. The effectiveness of the spiral ribs ranged from 1.3 to 1.4, and from 1.2 to 1.4 for the transverse ribs, spanning Re values from 60,000 to 400,000. These data include variations introduced by alternate transformation methods that were used to make annulus test results applicable to rod geometry.

The surfaces investigated in these tests were considered for fast gas-cooled reactors; however, the range of parameters studied also applies to heat transfer from ribbed rod-type fuel elements in thermal gas-cooled reactors.

1. INTRODUCTION

The performance of gas-cooled reactors is often limited by the heat transfer in the reactor core. One direct method for increasing the heat transfer rates is to raise the flow velocity; however, any gain is quickly

lost to the more rapid rise in pumping power. Hence, a more profitable approach lies in the search for ways to modify the flow and/or the surface in order to enhance the heat transfer without an excessive increase in the pressure drop. Studies in these directions^{1,2} have been underway at the Oak Ridge National Laboratory for several years, and a test facility has been developed capable of investigating the heat transfer behavior of a variety of tube and rod surfaces in gaseous flow at pressures up to 1000 psig and temperatures up to about 1200°F.

The objective of the present test was to study the heat transfer and pressure drop characteristics of specific enhanced heat transfer surfaces considered by General Atomics³ for potential use in advanced fast gas-cooled reactors. Cylindrical rod surfaces, photoetched by GGA to produce external ribs, were to be tested in annular geometry using nitrogen gas at pressures up to 400 psig as coolant, with surface temperatures to reach up to 1400°F at linear heat ratings up to three kW/ft. Under these conditions the nitrogen tests (expressed in terms of a nondimensional relationship of the Nusselt modulus as a function of the Reynolds and Prandtl moduli), would simulate thermally and dynamically the heat transfer and flow for high performance helium-cooled reactors that might operate in the pressure range from 1000 to 1200 psig with linear heat ratings up to 14 kW/ft and wall temperatures reaching 1400°F.

2. EXPERIMENTAL EQUIPMENT AND PROCEDURES

2.1 Test Facility

A schematic arrangement of the test equipment for once-through operation with either helium or nitrogen gas at up to 1250 psig pressure is shown in Fig. 2.1. For clarity not all thermocouples are pictured. In the present series of tests, the coolant was nitrogen gas supplied from a trailer truck that contained up to 2400 lb_m at 1600 psig.

The gas pressure in the flow channel was controlled by a pressure regulator located upstream of the gas preheater. Most of the runs were conducted at about 200 psig; a number of runs, primarily those at higher flow rates, were run at 400 psig. The gas flow rates were measured using

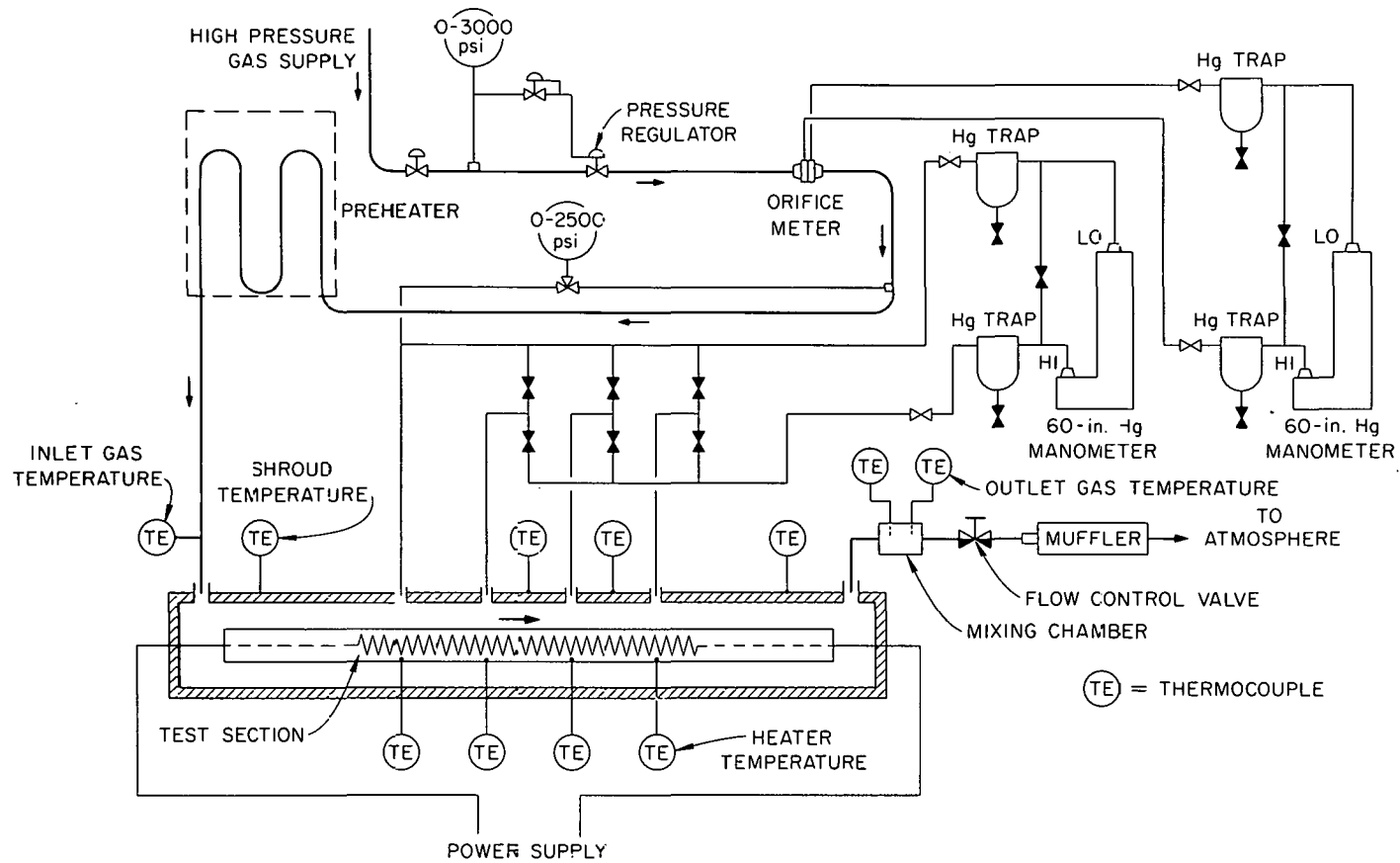


Fig. 2.1. Test facility schematic diagram.

an ASME type orifice meter that had been calibrated over the range 0.01 to 0.13 lb_m/sec at 200 psig nitrogen gas pressure using three Fisher-Porter rotameters. The rotameters in turn had been calibrated with a positive displacement meter that showed them to be accurate and precise to within $\pm 1\%$. The orifice meter pressure and the test channel pressure were obtained with a 0 to 2500 psig Heise gage. The pressure drop across the 0.437-in. ID sharp-edged orifice of the flowmeter and between the pressure taps along the heated length of the flow channel was obtained with a Series 500 Exactel Servomanometer designed to measure pressure drops of up to 60 in. to within ± 0.004 in. over the full range of system pressure.

Downstream of the orifice meter the gas entered an ohmically heated preheater (150 kW capacity) connected to two saturable reactors in parallel, which supplied an alternating current at up to 30 V. The preheater exit temperature, which ranged from ambient up to 760°F, was measured by two chromel-alumel thermocouples inserted into the gas stream. From the preheater, the gas flowed into the pressure shell that housed the test section. As shown in Fig. 2.2, each heater rod was located inside a flow shroud in concentric annular flow geometry. Streamlined centering spacers were brazed to each heater rod at 120-deg azimuthal intervals at the axial positions shown in Fig. 2.2. The test section was set vertically in order to minimize deflection of the heaters. Examination of the heating surfaces after completion of the tests gave no indication of misalignment. The shroud, depicted in Fig. 2.3, consisted of a 304 SS tube, 0.600-in.-ID and 0.065-in.-wall thickness. Gas pressure drop measurements in the heated region were obtained from 0.030-in.-ID holes provided in the shroud wall at 90-deg azimuthal intervals at each of four axial positions abreast of the heater rod thermocouples (see Fig. 2.2). The pressure shell, depicted in Fig. 2.4, was designed to accommodate shrouds containing rod clusters with up to seven heaters. The void space between the flow shroud and the pressure shell and also the exterior surface of the pressure shell were insulated thermally with Kaowool. The coolant gas entered the pressure shell at four circumferential points 90 deg apart in order to promote azimuthal flow symmetry. The flow was dispersed further by a perforated baffle through which the gas passed before it entered the

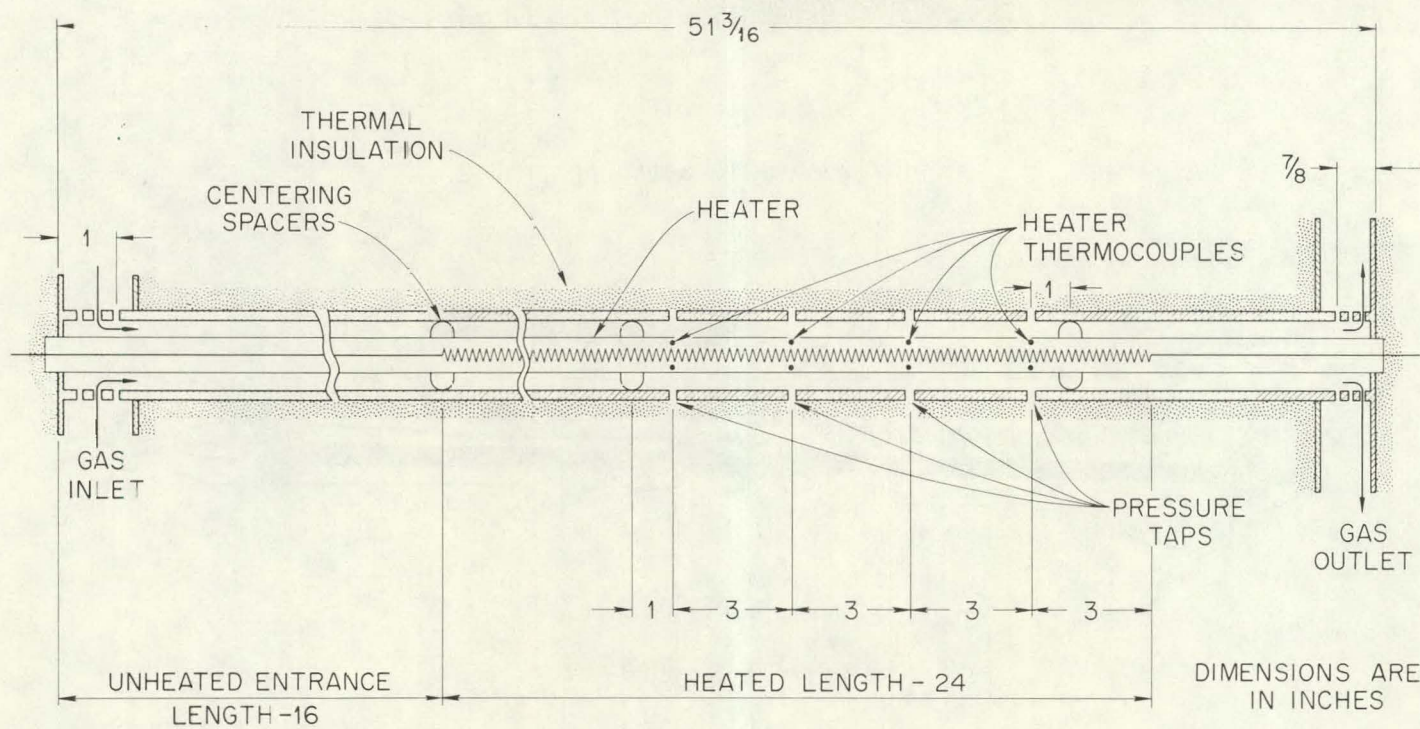


Fig. 2.2. Test channel arrangement.

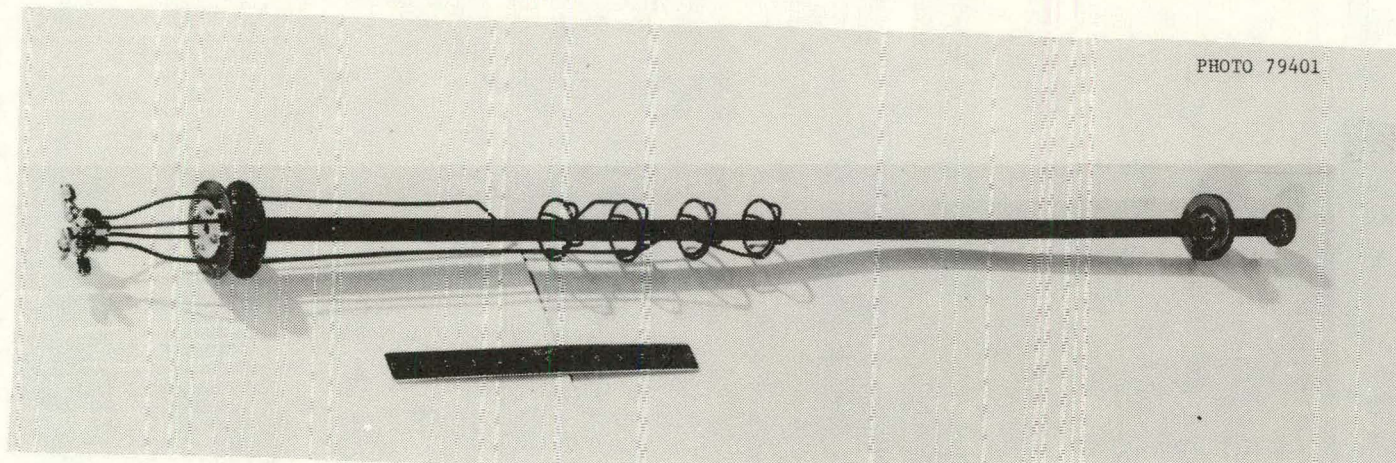


Fig. 2.3. View of flow shroud.

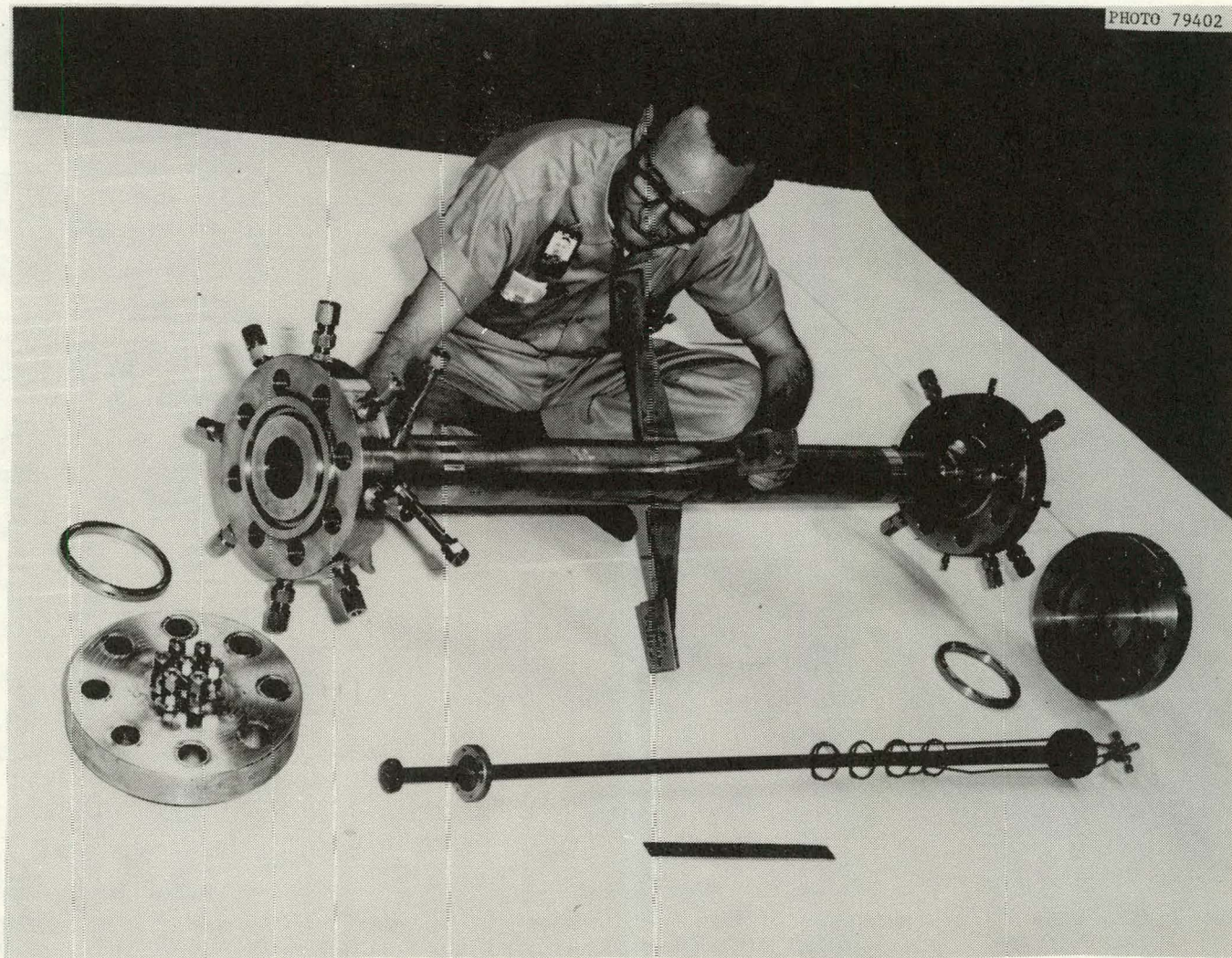


Fig. 2.4. View of pressure shell and flow shroud.

annulus. The flow arrangement at the exit to the annulus was similar. The exit region of the test assembly before the application of insulation is depicted in Fig. 2.5. Chromel-alumel thermocouples spotwelded to the exterior of the flow shroud and the pressure shell were used to obtain the temperatures needed to determine the heat loss to the environment. The gas exit temperature was measured with a sheathed chromel-alumel thermocouple inserted into the flow downstream of a mixing section to assure a good mixed mean temperature.

Signals from the thermocouples employed in the test were displayed on four multipoint Brown recorders and on two two-point line recorders. Electrical power for the heater rod was supplied from four stacked variacs with a capacity of 24 kW at 200 volts ac. The voltage across the test section was measured with a Fluke digital voltmeter accurate to within $\pm 0.05\%$. The current was read from a precision Weston ammeter accurate to within $\pm 0.75\%$ that was fed by a 20:1 current transformer.

2.2 Heater Rods

The heater rods manufactured⁴ by the Watlow Electric Manufacturing Company of St. Louis, Missouri, were dimensionally prototypic of nuclear fuel rods considered for use in advanced gas-cooled fast breeder reactors. The 2-ft-long heated section consisted of a closely wound helical coil of Nichrome-V wire located concentrically within the 304 SS heater sheaths and separated from them by compacted boron nitride. Each end of the heating coil was connected to a 0.125-in.-OD copper lead-in conductor. Eight sheathed and grounded type K chromel-alumel thermocouples of 0.020 in. OD were located in four 0.020-in. by 0.020-in. axial grooves machined 90 deg apart on the outer periphery of the 0.037-in.-thick inner sheath. The thermocouples were held in place by a 0.012-in.-thick outer sheath swaged onto the inner sheath. The thermocouples were arranged to provide two diametrically opposite measuring points at each of the four axial locations shown in Fig. 2.2. Each pair of thermocouples was oriented 90 deg apart azimuthally from the adjacent pair. The sheath thermocouples were located well within the heated length so that temperature measurements would be unaffected by end losses. Examination of heater radiographs revealed that the heater coil eccentricity did not exceed 0.015 in. and the variation in the number of coils per inch was generally

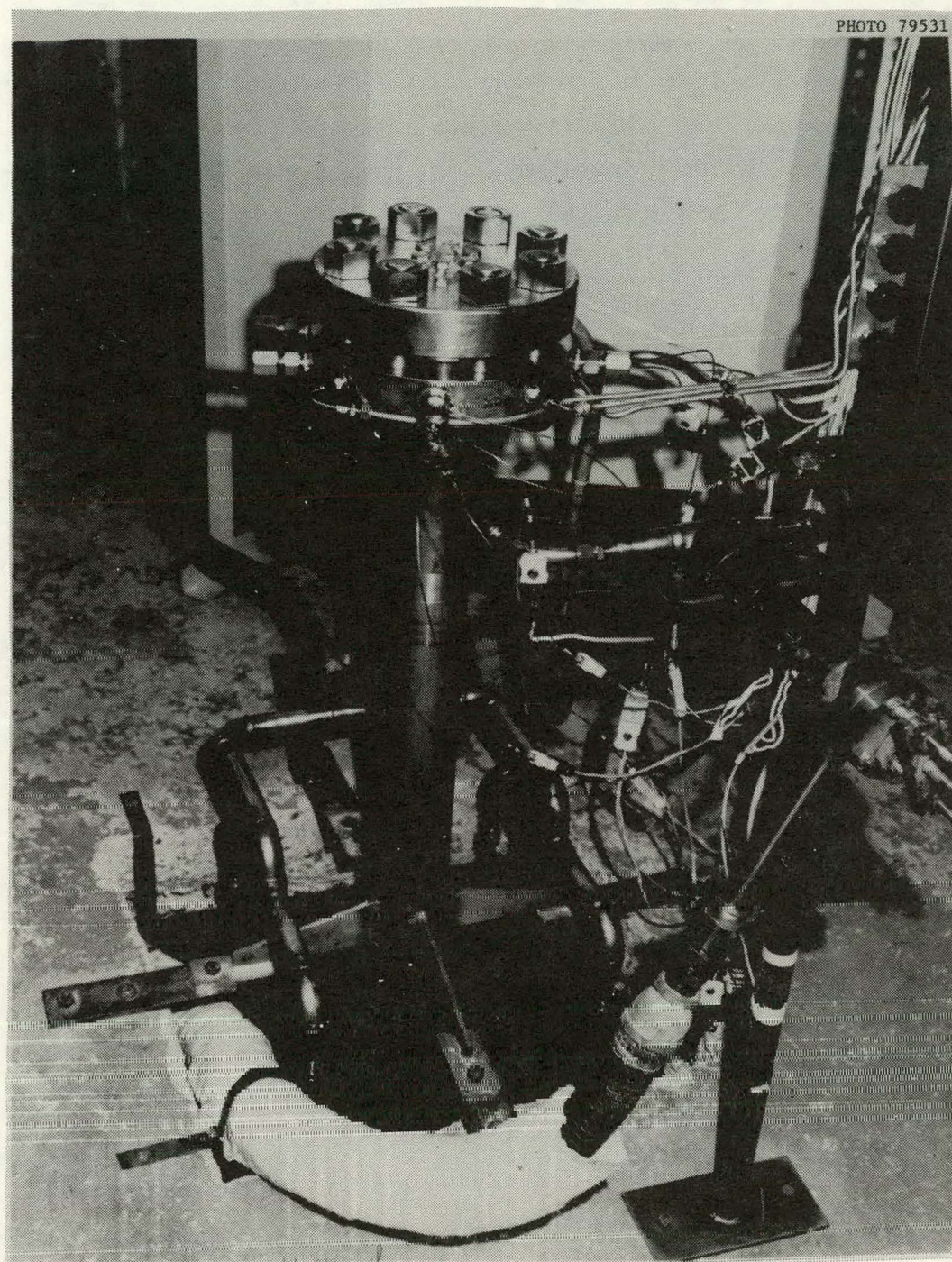


PHOTO 79531

Fig. 2.5. View of test assembly in place.

less than $\pm 1\%$; it was estimated that these discrepancies would not perturb the uniformity of the heat flux significantly. The heat flux distribution of the heaters was also checked⁵ using a high-speed scanning infrared camera. In those tests an electric current was passed through the heating coil under steady-state and transient conditions while the heater surface temperatures were scanned for nonuniformity. A heating current was also applied to the heater sheath during a transient test to determine local temperature peaks resulting from poor contact between the sheath and the boron nitride insulation. The results of the scanning tests suggested that the heat flux distribution of the heater rods would be satisfactory.

Three heaters with different surfaces were tested. Heater rod A had a smooth exterior surface of 0.302 in. OD. The surface of heater B depicted in Fig. 2.6 was photoetched to within about 2 in. of each end to produce helical fins 0.006 in. high and 0.012 in. wide with a pitch of 0.072 in. and a helix angle of 37 deg. The fin dimensions were fairly uniform although the fillet radius at the fin base varied somewhat from place to place. The etched surfaces did not appear as smooth as the original rod surface. This was confirmed with surface roughness measurements performed with a profilometer, which showed a roughness of 40 to 65 μrms for the etched surfaces vs 15 to 20 μrms for the original surface. The outside diameter of the heater was 0.289 in. excluding the height of the fins. Heater C was roughened by the same technique to produce fins of approximately the same height, width, and spacing, but in ring geometry instead of a helical configuration. As depicted in Fig. 2.7, the degree of fin shape uniformity and surface roughness appears similar to those observed for heater B. The outside diameter was 0.288 in.

2.3 Test Conditions

The testing program was designed to measure the heat transfer and pressure drop characteristics of the various surfaces under steady-state conditions. Test conditions were considered sufficiently stable if system temperatures and flow rates did not change more than about 1% while

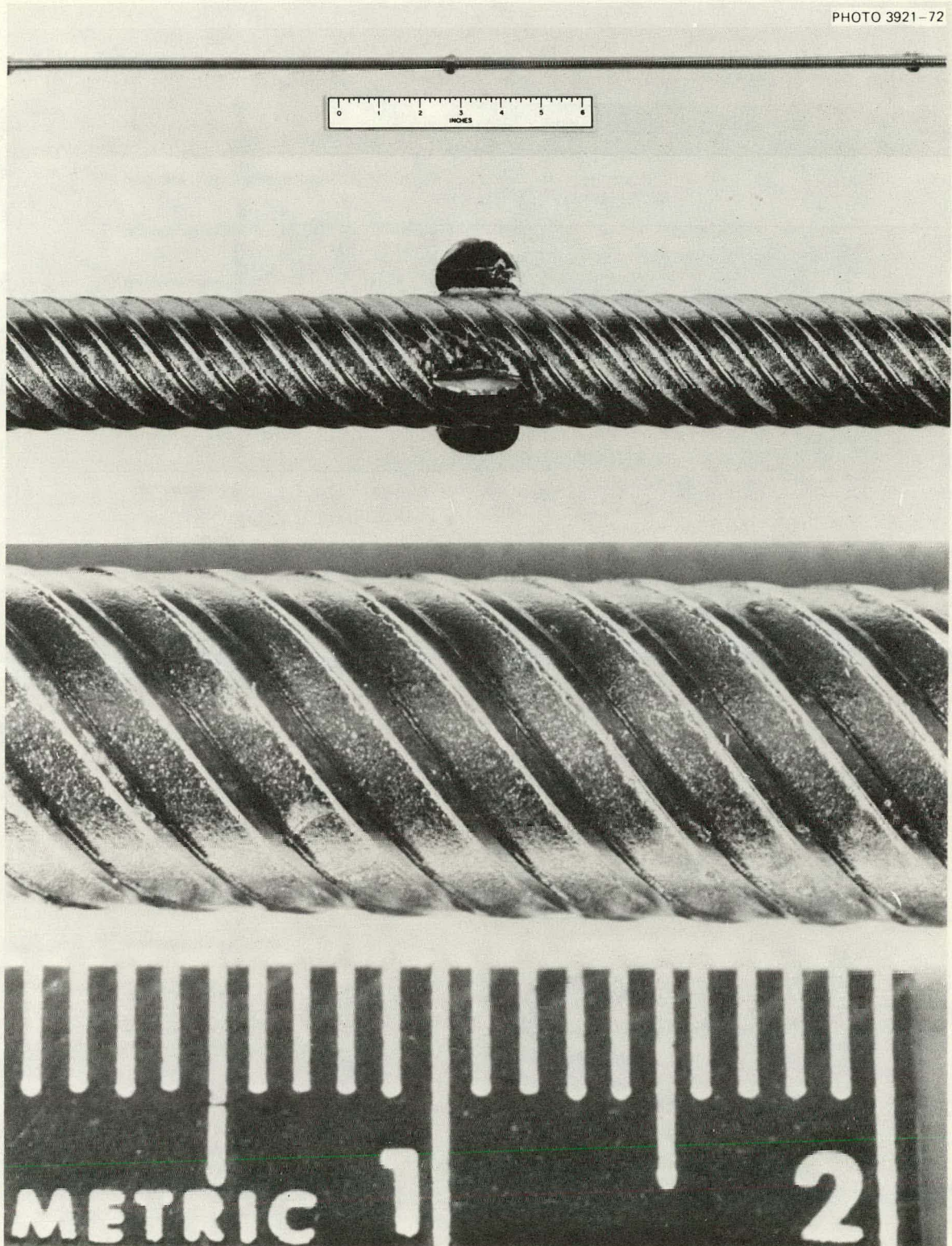


Fig. 2.6. View of helically ribbed surface, heater B.

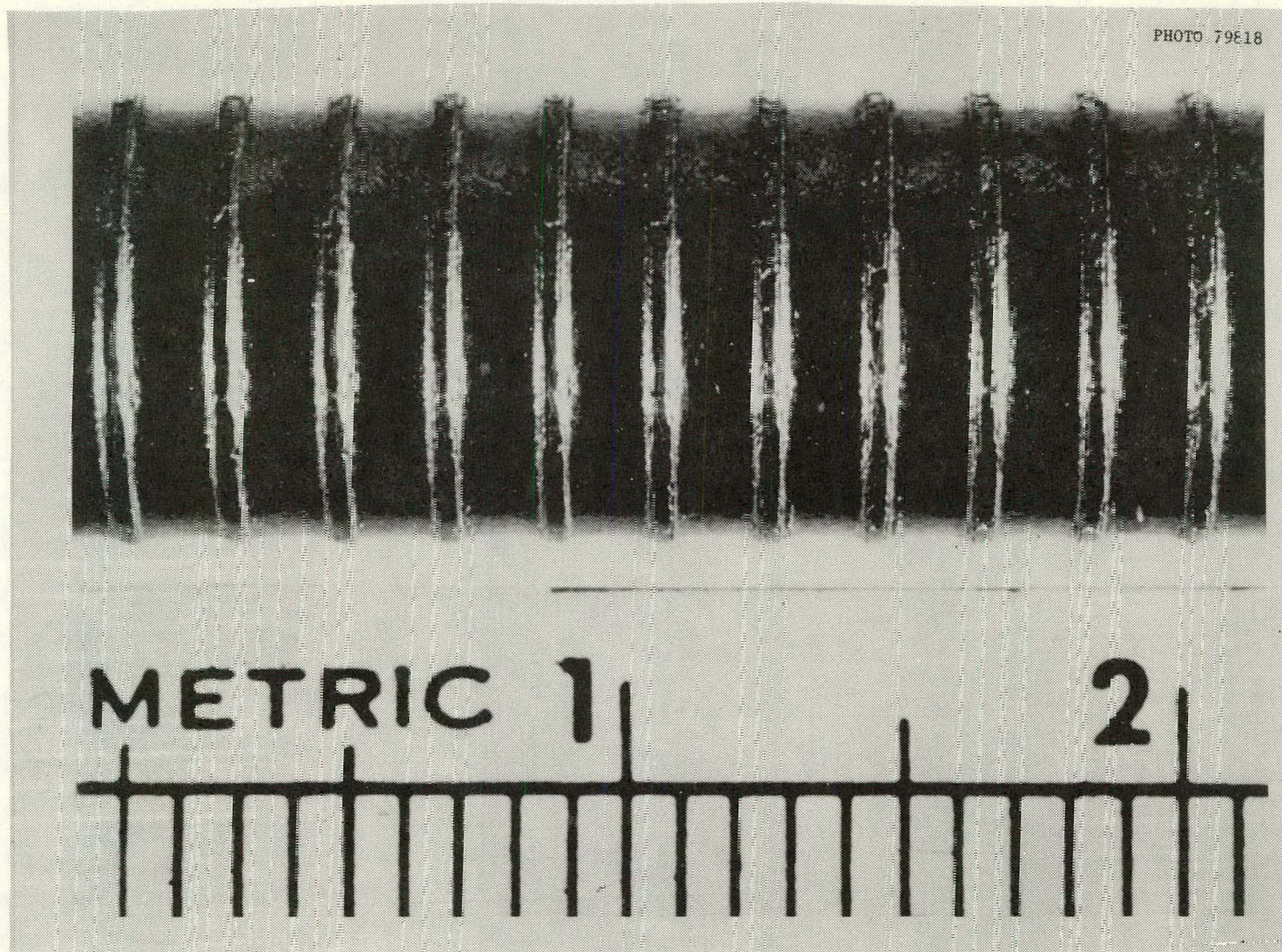


Fig. 2.7. View of transversely ribbed surface, heater C.

the data were being recorded, involving a time period of five to ten minutes duration. Because of its mass and associated thermal inertia, the gas preheater required a two to three hour warmup period before stable operation could be achieved. The test sequence was planned to minimize the variation of gas inlet, gas outlet, and peak heater surface temperatures between successive runs in order to reduce the time required to approach steady state.

About 170 test runs were completed including 38 tests to determine heat losses and adiabatic pressure drops. The linear heat rates reached were 4.4, 6.7, and 6.8 kW/ft, respectively, for heaters A, B, and C. This was well below the peak design capability of 12 kW/ft available for tests possibly using helium gas as a coolant. The peak power delivered by the preheater was 21.1 kW; gas flow rates ranged from 0.01 to 0.2 lb_m/sec. The Reynolds moduli reached up to 450,000 and heat fluxes reached values in excess of 300,000 Btu/hr·ft² at surface temperatures up to 1400°F. The test section gas exit temperature reached 1100°F and T_w/T_b ranged from 1.2 to 2.4.

3. DATA REDUCTION AND TRANSFORMATIONS

3.1 Heat Transfer Calculations

A computer program written in FORTRAN IV and listed in Appendix A was used to analyze the heat transfer and pressure drop measurements obtained during the tests. For purposes of calculation, the test length was divided into seven axial segments. Three of these segments were located in the instrumented region of the heater rod with their boundaries coinciding with the heater thermocouple locations (see Fig. 2.2).

The heat transfer computation was begun by performing a heat balance over the test section. The energy gained by the gas (as inferred from the gas flow and the gas temperature rise) and the heat lost through the insulation was summed and compared with the electrical energy supplied to the experiment. Runs with a discrepancy greater than 5% were discarded. The electrical conductivity of the Nichrome heating coil, and consequently its heat generation rate, was assumed uniform along the heated length,

introducing a potential error of less than 0.7% in the value of the heat flux. The rate of gas energy gain in each segment was calculated from:

$$Q_g = Q_e - Q_\ell , \quad (3.1)$$

where Q_e is the rate of electrical heat generation and Q_ℓ is the loss through the insulation. The gas enthalpy rise was calculated from:

$$\Delta H = Q_g / W , \quad (3.2)$$

where W is the mass flow rate. The local gas enthalpies were determined by adding the enthalpy rise in each segment. The local gas pressure was calculated from measurements in the flow channel assuming linear pressure variation, thus determining the gas state in each segment. The properties of nitrogen gas were computed from two computer subprograms, TABHP and TABTP taken from Ref. 6.

The heater sheath temperatures were measured by thermocouples located in the inner sheath. The outer surface temperatures were then determined by calculating the radial temperature gradient assuming a uniform heat flux. The thermal conductivity of the sheath material was based on the local temperature.

Having determined the local gas and surface temperatures as well as the local gas energy gain, the calculation of heat transfer coefficients and various nondimensional groupings was straightforward.

3.2 Friction Factor Calculations

For analyzing the pressure drop measurements, each test section was analytically divided into three segments with boundaries defined by the location of the pressure taps as shown in Fig. 2.2.

The computer calculations of the experimental friction factors and associated parameters used gas properties obtained in the heat transfer analysis. The observed pressure drops were corrected to remove contributions from changes in axial flow velocity. Accelerations were due to changes in gas density and in channel flow area; thus:

$$\Delta P_{\text{friction}} = \Delta P_{\text{measured}} - \Delta P_{\text{density}} - \Delta P_{\text{flow area}} \quad (3.3)$$

The pressure drop due to density change was calculated by Eq. (3.4) taken from Ref. 7:

$$\Delta P_{\text{density}} = \frac{G^2}{g_c} \left(\frac{1}{\rho_2} - \frac{1}{\rho_1} \right), \quad (3.4)$$

where the subscripts 1 and 2 refer to the entrance and exit, respectively, of the region considered. Slight changes in channel flow area were caused by diametral (<0.004 in.) shrinkage of the flow shroud at the pressure taps during fabrication. The corresponding pressure drops were calculated as follows from Ref. 7:

$$\Delta P_{\text{flow area}} = \frac{G^2}{2g_c \rho} [1 - (A_1/A_2)^2], \quad (3.5)$$

where A_1 and A_2 are the cross-sectional areas preceding and following the area change.

The Blasius friction factor was determined from:

$$f = \frac{2g_c D_h}{\rho_I \bar{V}^2 (X_2 - X_1)} \Delta P_{\text{friction}} \quad (3.6)$$

Here \bar{V} is the average gas bulk velocity in the segment under consideration and X is the axial position along the heater rod where the subscripts 1 and 2 correspond to the entrance and exit of a segment. Following the recommendations of Ref. 8, the gas properties entering into the friction factor f and the modified Reynolds modulus Re_I were evaluated at an effective temperature T_I given by:

$$T_I = B (T_w - T_b) + T_b \quad (3.7)$$

The value of $B = 0.05$ was selected by trial and error to remove data scatter resulting from temperature dependent gas property variations.

3.3 Transformations

The measurements obtained in these tests reflect the influence of both the rod surface and the shroud surface. Thus, for example, increasing the roughness of the rod surface would improve the measured heat transfer coefficient while the friction factor would increase a relatively small amount since the character of most of the wetted perimeters, namely the shroud surface, has not changed. Consequently, it would be incorrect to apply the average heat transfer coefficients and friction factors obtained from an annulus experiment to a bundle type reactor fuel element in which most of the surface would be roughened, and it becomes necessary to separate the contributions from the component surfaces. In recent years, most of the methods to accomplish this separation have relied on the principle of a transformation due to Hall.⁹ These methods have made use of a surface of zero shear for separating the properties of the rough and the smooth surfaces, but they differ in the method for locating it. With the present state of knowledge, experimental measurements are required to locate the zero-shear surface precisely; however, these measurements are difficult to perform, and a number of simplified methods have been used to estimate the surface's position.

In the present study a Hall-type transformation recommended by Markóczy¹⁰ on the basis of experimental verification in Ref. 11 was used to remove the effect of the shroud surface upon the Stanton modulus and the friction factors of the rod heaters. Additionally, this particular transformation should allow direct comparison in the future with heat transfer tests on similar surfaces underway at the Eidg. Institut für Reaktorforschung in Würenlingen, Switzerland. In the transformation, the annulus is assumed to consist of two concentric flow regions separated by an adiabatic zero-shear surface, as depicted in Fig. 3.1. Below are listed some of the assumptions used in the development of the friction factor and Stanton modulus transformations.

1. The axial pressure drop is uniform in the flow regions.
2. The surface heat flux is uniform and the fluid temperature profiles are fully developed, thus $\partial T / \partial X$ is constant.
3. The fluid properties are independent of radial position.

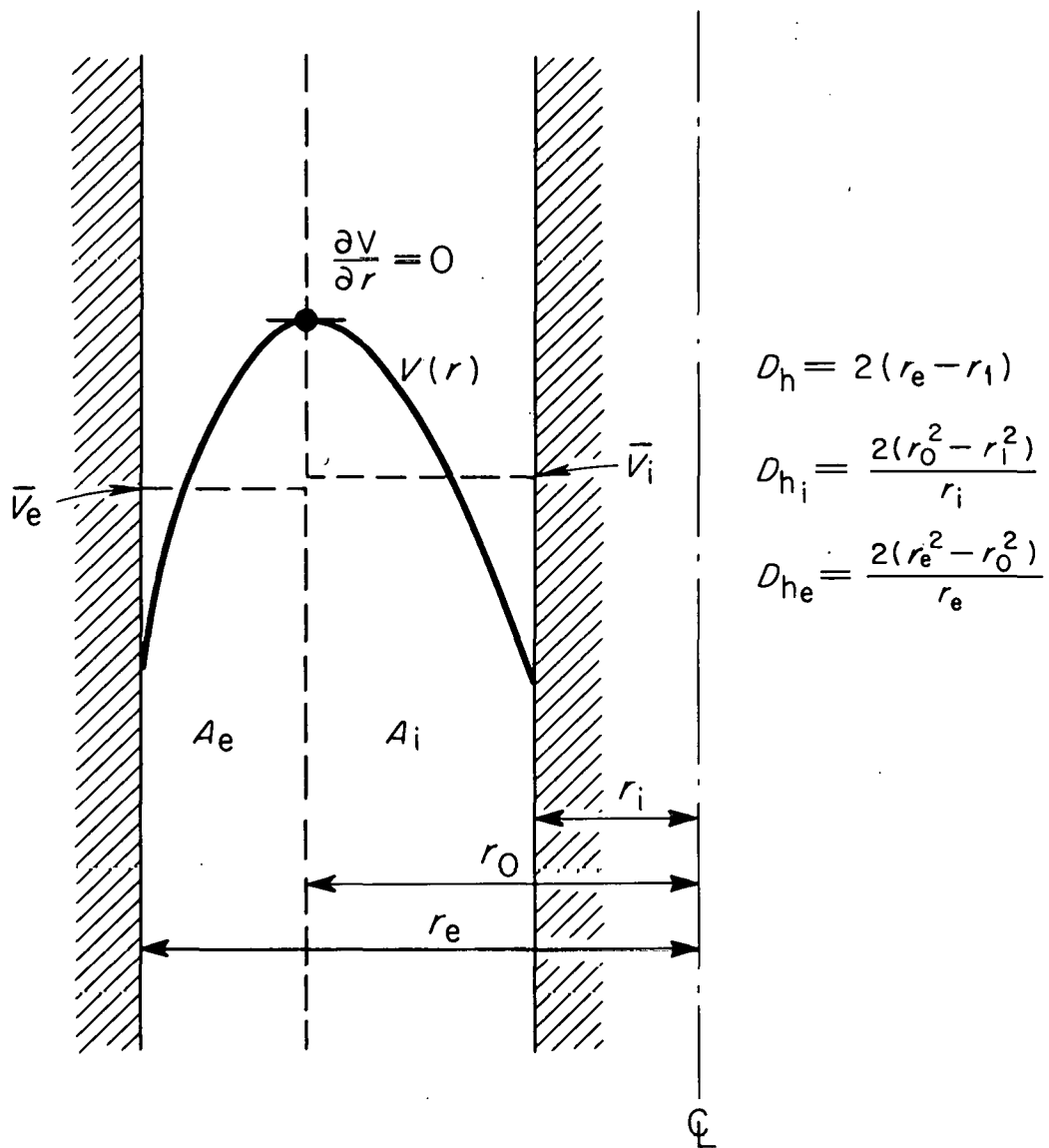


Fig. 3.1. Annulus flow channel diagram.

4. The effective conductivity, K , of the gas in the turbulent region is independent of the radial temperature distribution.

5. The surfaces of zero shear and maximum velocity coincide. This ignores radial velocity components that are probably minor.

6. The rod surface heat flux \dot{q} is identical for the experimental and transformed cases, thus, $\dot{q} = \dot{q}_i$.

7. For the transformed case there is no momentum or heat transport across the surface of zero shear.

8. There is no interaction between the velocity and the temperature distribution.

9. The average velocities in the inner and the outer channel are the same, thus $\bar{V}_i = \bar{V}_e = \bar{V}$.

The actual test conditions probably do not satisfy the stipulated physical conditions. However, this does not detract from the usefulness of the approach, since it leads to relatively simple analytical solutions to complex problems, providing a convenient method for correlating and applying a variety of experimental data on rod-type heat transfer surfaces.

3.3.1 Friction Factor Transformation

The subscript i has been used to identify the inner channel while e designates the outer channel; nonsubscripted symbols refer to the entire flow area. Under the first assumption:

$$\frac{\partial P}{\partial X} = \frac{\partial P_i}{\partial X} = \frac{\partial P_e}{\partial X} . \quad (3.8)$$

Thus, under Assumptions (3) and (9) one obtains:

$$\frac{f_i}{f} = \frac{D_{hi}}{D_h} , \quad (3.9)$$

and

$$\frac{f_e}{f} = \frac{D_{he}}{D_h} . \quad (3.10)$$

As indicated in Fig. 3.1, the hydraulic diameters of the various flow channels are given by the expressions:

$$D_h = 2(r_e - r_o); \quad D_{h_i} = \frac{2(r_o^2 - r_i^2)}{r_i}; \quad D_{h_e} = \frac{2(r_e^2 - r_o^2)}{r_e}.$$

Defining:

$$D_h \equiv \frac{4A}{p}; \quad D_{h_i} \equiv \frac{4A_i}{p_i}; \quad D_{h_e} \equiv \frac{4A_e}{p_e} \quad (3.11)$$

and

$$A^* \equiv \frac{A_e}{A}; \quad p^* \equiv \frac{p_e}{p}, \quad (3.12)$$

one can obtain from Eqs. (3.9) and (3.10):

$$\frac{f_i}{f} = \frac{1 - A^*}{1 - p^*}; \quad \frac{f_e}{f} = \frac{A^*}{p^*}. \quad (3.13)$$

From the definition of the Reynolds modulus and Assumptions (3) and (9), it follows that:

$$\frac{Re_i}{Re} = \frac{D_{hi}}{D_h}; \quad \frac{Re_e}{Re} = \frac{D_{he}}{D_h}. \quad (3.14)$$

Substituting Eqs. (3.9) and (3.10), respectively, one obtains:

$$\frac{Re_i}{Re} = \frac{f_i}{f} \text{ and } \frac{Re_e}{Re} = \frac{f_e}{f}. \quad (3.15)$$

Assuming that the friction factor of the smooth outer channel can be represented by:

$$f_e = C Re_e^n, \quad (3.16)$$

and taking Eq. (3.13) into account it follows that:

$$f = C \operatorname{Re}_e^n \frac{p^*}{A^*}, \quad (3.17)$$

and

$$\frac{\operatorname{Re}_e}{\operatorname{Re}} = \frac{f_e}{f} = \frac{A^*}{p^*}. \quad (3.18)$$

Letting f_s be the friction factor for the entire flow channel with smooth surfaces at a Reynolds modulus of Re , one obtains

$$\frac{f}{f_s} = \frac{C \operatorname{Re}_e^n p^*}{C \operatorname{Re}^n A^*}. \quad (3.19)$$

Substituting Eq. (3.18), it follows that:

$$\frac{f}{f_s} = \left(\frac{A^*}{p^*} \right)^{n-1}, \quad (3.20)$$

and solving for A^* :

$$A^* = p^* \left(\frac{f}{f_s} \right)^{1/(n-1)} \quad (3.21)$$

Combining Eqs. (3.13) and (3.21) one obtains:

$$\frac{f_i}{f} = \frac{1 - p^* (f/f_s)^{1/(n-1)}}{1 - p^*}. \quad (3.22)$$

Here f_i is the friction factor for a rod surface surrounded by a flow annulus, which in turn is bounded by a zero-shear surface at r_o . In principle these values no longer reflect the influence of the outer wall of the test annulus, thus allowing comparison with and application to other flow geometries that have been similarly transformed.

If the friction factor, f_s , is known, the position of the surface of zero shear can be computed from (3.21):

$$r_o = \sqrt{r_e^2 - (r_e - r_i) r_e (f/f_s)^{1/(n-1)}}. \quad (3.23)$$

For smooth surfaces this reduces to:

$$r_o = \sqrt{r_i r_e}. \quad (3.24)$$

3.3.2 Stanton Modulus Transformation

3.3.2.1 Hall-Type Transformation. The ratio of the Stanton modulus transformed for a rod, St_i , to that observed for tests with annular geometry, St , is given by:¹¹

$$\frac{St_i}{St} = \frac{\frac{(T_w - T_b) k f_i \bar{V}}{8 v \dot{q}}}{\left(\frac{\Delta \bar{T} k f_i \bar{V}}{8 v \dot{q}} - 1 \right) \frac{\phi(r_e/r_i)}{\phi(r_o/r_i)} + 1}, \quad (3.25)$$

where

$$\phi(r_e/r_i) = \frac{[(r_e/r_i)^2 - 1]^2}{(r_e/r_i)^4 [4\eta(r_e/r_i) - 3] + 4(r_e/r_i)^2 - 1} \quad (3.26)$$

and

$$\phi(r_o/r_i) = \frac{[(r_o/r_i)^2 - 1]^2}{(r_o/r_i)^4 [4\eta(r_o/r_i) - 3] + 4(r_o/r_i)^2 - 1}. \quad (3.27)$$

The radius r_o of the zero-shear surface in Eq. (3.25) was obtained from Eqs. (3.23) and (3.24). The rod surface heat flux, the effective turbulent conductivity of the gas, and the average gas flow velocities are the same for the transformed and experimental case in accordance with Assumptions 6, 8, and 9. The velocity was assumed constant across the flow channel except in the sublayer at the wall.

3.3.2.2 Wilkie's Transformation. An alternative transformation for the Stanton modulus is one recommended by Wilkie^{1,2} for square and other rib profiles:

$$\frac{St_i}{St} = 1.61 - 0.8 A_i/A . \quad (3.28)$$

Here A_i is the cross-sectional flow area between the rod surface and the zero-shear diameter D_o . In the present analysis, D_o was obtained from Eq. (3.23). Equation (3.28) is an empirical relationship based on over 200 experimental points, and it applies to annuli with a smooth to rough perimeter ratio of about 2, to gases with $Pr = 0.7$, and T_w/T_o between 1.19 and 1.25. Equation (3.28) was therefore judged applicable to the subject tests.

4. RESULTS AND DISCUSSION

4.1 Pressure Drop Results

Before entering the test annulus, the coolant gas traverses a 45-diam-long unheated entrance region, sufficient^{1,3} for the velocity profile to approach full development. The pressure drop measurements within the heated length were made at points beyond the rod centering spacers, at least 40 diameters into the heated region. Entrance length data for the flow of air in tubes^{1,4} suggests this to be adequate to establish thermally and hydrodynamically developed flow. This expectation was confirmed by local friction factors, which were observed to be generally uniform. Pressure drop results for isothermal and heated tests are shown in terms of the annulus friction factor f , Eq. (3.6), in Fig. 4.1. Use of Eq. (3.7) to determine the gas properties removed data scatter due to temperature dependent properties. Also depicted is a friction factor relationship recommended by Knudsen and Katz^{1,5} for smooth annuli:

$$f = 0.2052 Re^{-0.2} , \quad (4.1)$$

showing reasonably good agreement. EIR¹⁶ results obtained with air at low pressure for $r_e/r_i = 2.09$ at relatively low Re values agree quite well. The present results for a smooth annulus are well represented by:

$$f = 0.118 \text{ Re}^{-0.155} \quad (4.2)$$

The largest friction factors were obtained for the surface with ring-type ribs while the rod with helical ribs gave values about midway between smooth and ring-type rib results. It can be seen in Fig. 4.1 that as the effective surface roughness increases, the friction factors show diminished dependence on the Reynolds modulus. This behavior is consistent with that observed for flows inside of roughened tubes.¹⁷

Figure 4.2 depicts the isothermal and the heated rod friction factors f_i , as calculated by Eq. (3.6) and transformed by Eq. (3.22) to remove the effect of the annulus outer wall. Good agreement with Wilkie's isothermal data¹⁸ for smooth rods is apparent in Fig. 4.2. It will be noted that rod friction factors exceed the annulus friction factors of Fig. 4.1 by about 50% for the helical ribs and 90% for the transverse ribs, indicating that in this instance, the transformation had a significant effect on the magnitude of the roughened rod friction factors. Friction factors for the annulus with only smooth surfaces were not changed by the transformation since in this instance $f_i/f = 1.0$ per Eq. (3.22).

At a Reynolds modulus of 100,000 the friction factors for the helical- and ring-ribbed rods exceeded the smooth rod values by about 115 and 260% respectively. The roughened rod friction factors showed less dependence on the Reynolds modulus than the corresponding annulus values; this is to be expected since the rod values apply to surfaces roughened over their entire area and thus characterized by an increased average roughness.

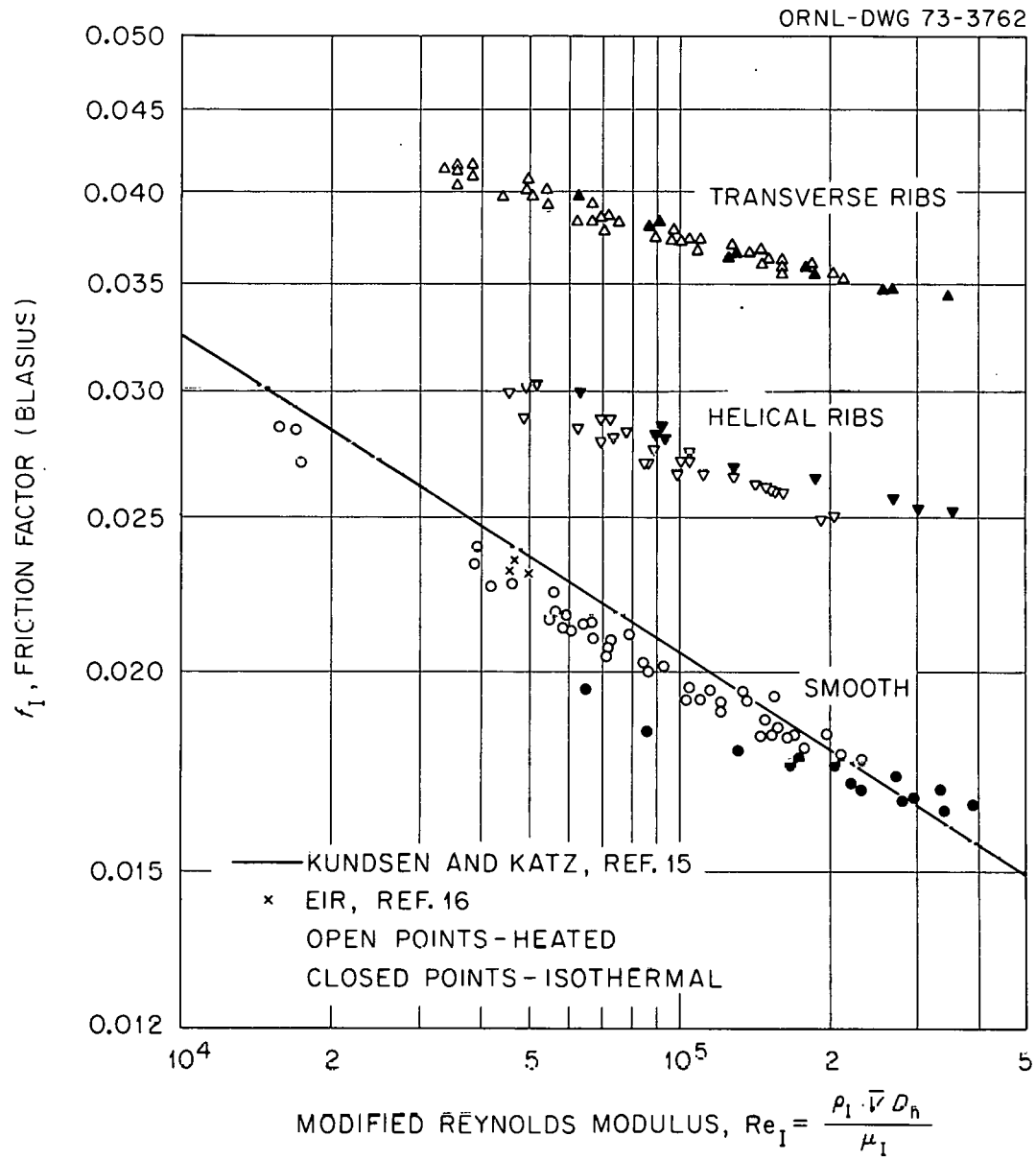


Fig. 4.1. Annulus friction factors.

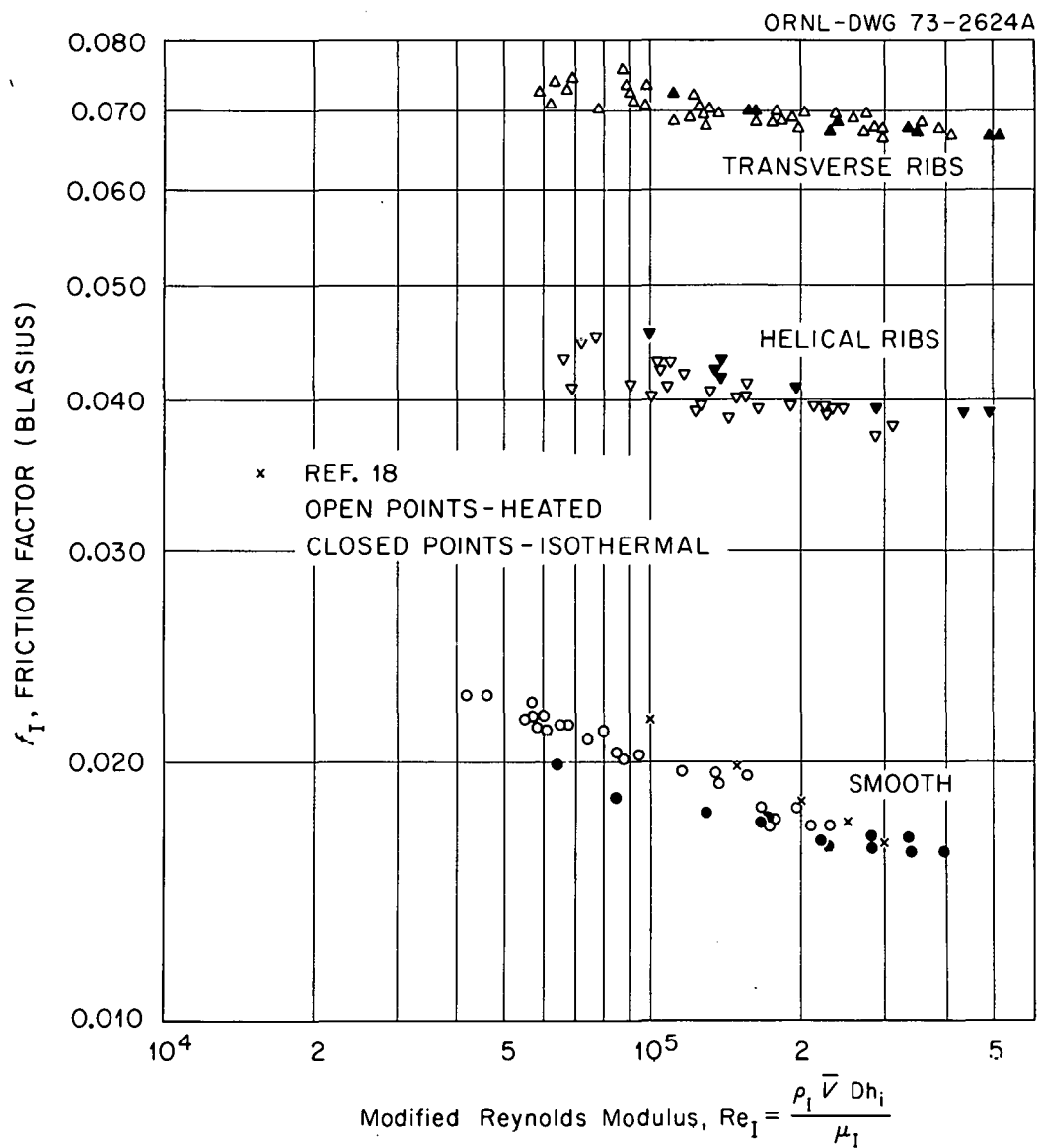


Fig. 4.2. Rod friction factors.

4.2 Heat Transfer Results

The heater rod temperatures were measured in a region extending from 40 to 80 diameters into the heated length. The heat transfer results presented are based on the average temperature of a 3-in.-long segment extending from 18 to 21 in. (60 to 70 hydraulic diameters) from the start of the heated length. The total entrance length was 113 hydraulic diameters (of which 45 diameters were unheated) sufficient according to smooth tube flow data¹⁴ to establish a fully developed temperature profile. This was validated by heat transfer measurements extending from 40 to 70 hydraulic diameters into the heated length, which showed an approach to uniform heat transfer coefficient values.

Annulus Stanton moduli for the three test surfaces are depicted in Fig. 4.3 plotted against the bulk Reynolds modulus; also shown are Kays¹⁹ results for smooth annuli that lie about 20% above the present smooth surface data. EIR's smooth surface results¹⁸ for $Re < 50,000$ lie about 35% above the present results. Figure 4.4 shows the results transformed by Eq. (3.25) into rod geometry. Also depicted are some of Wilkie's¹⁸ results for gaseous heat transfer. The solid line, representing his Stanton moduli for transverse ribs with a pitch to height ratio of 12 and a height to equivalent diameter ratio of 0.0106 (matching the subject test parameters), lies about 25% above the present results. Good agreement with Wilkie's smooth rod results (the dashed line in Fig. 4.4) is evident.

The data scatter of Figs. 4.3 and 4.4 was diminished considerably when those results were expressed in terms of $\phi(St)$, Figs. 4.5 and 4.6 where:

$$\phi(St) = St \, Pr^{0.6} (T_w/T_b)^n. \quad (4.3)$$

This form follows the recommendation of Kays;²⁰ a value of $n = 0.1$ limited the annulus data scatter due to temperature dependent property variations to a range of about $\pm 5\%$, compared to about $\pm 10\%$ for the Stanton modulus values. Data consistency was even better for the rod results, which show a scatter of only about 4% in Fig. 4.6 for ratios of wall-to-gas temperature ranging up to 2.4, and Reynolds moduli from about

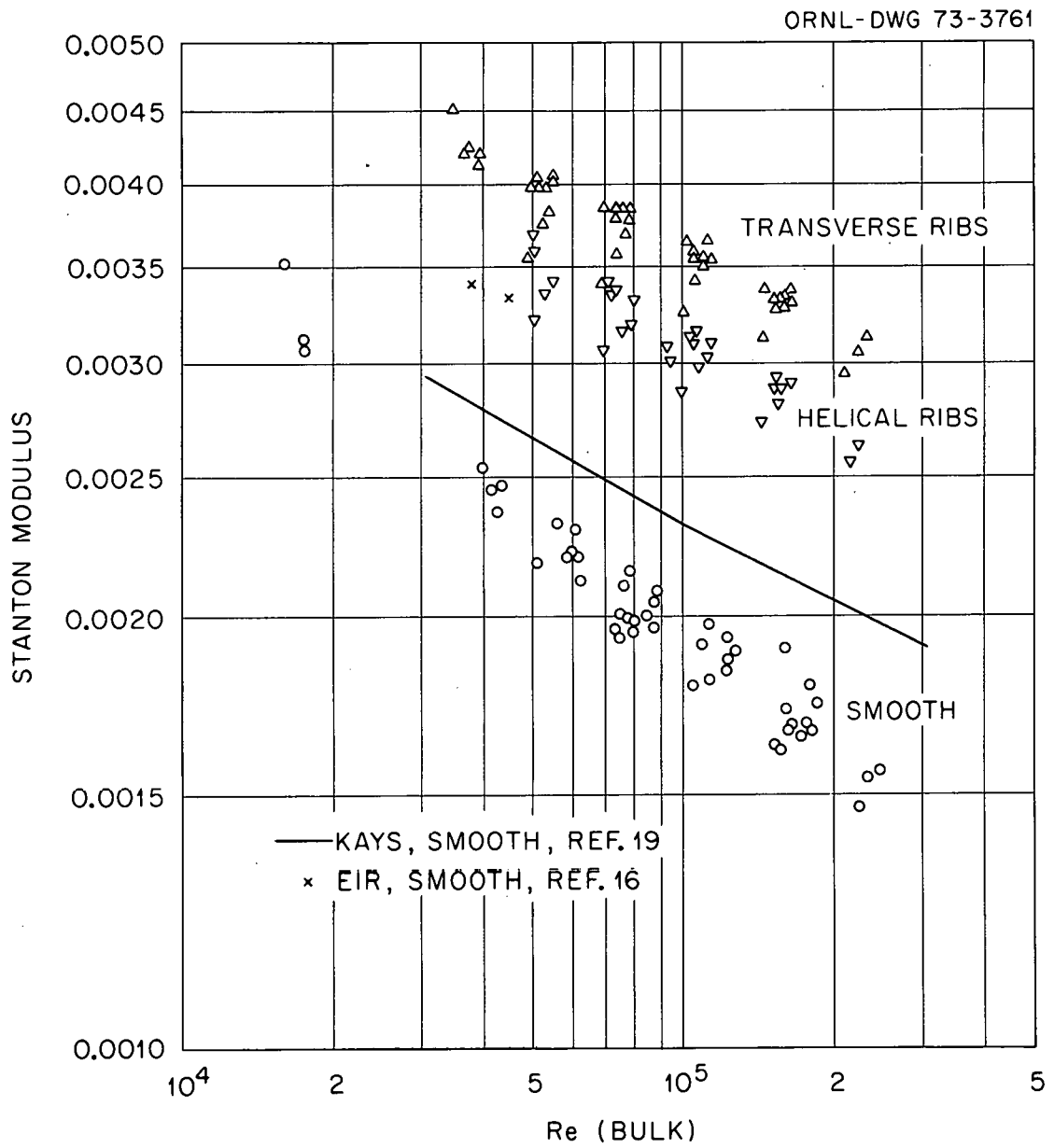


Fig. 4.3. Annulus Stanton modulus.

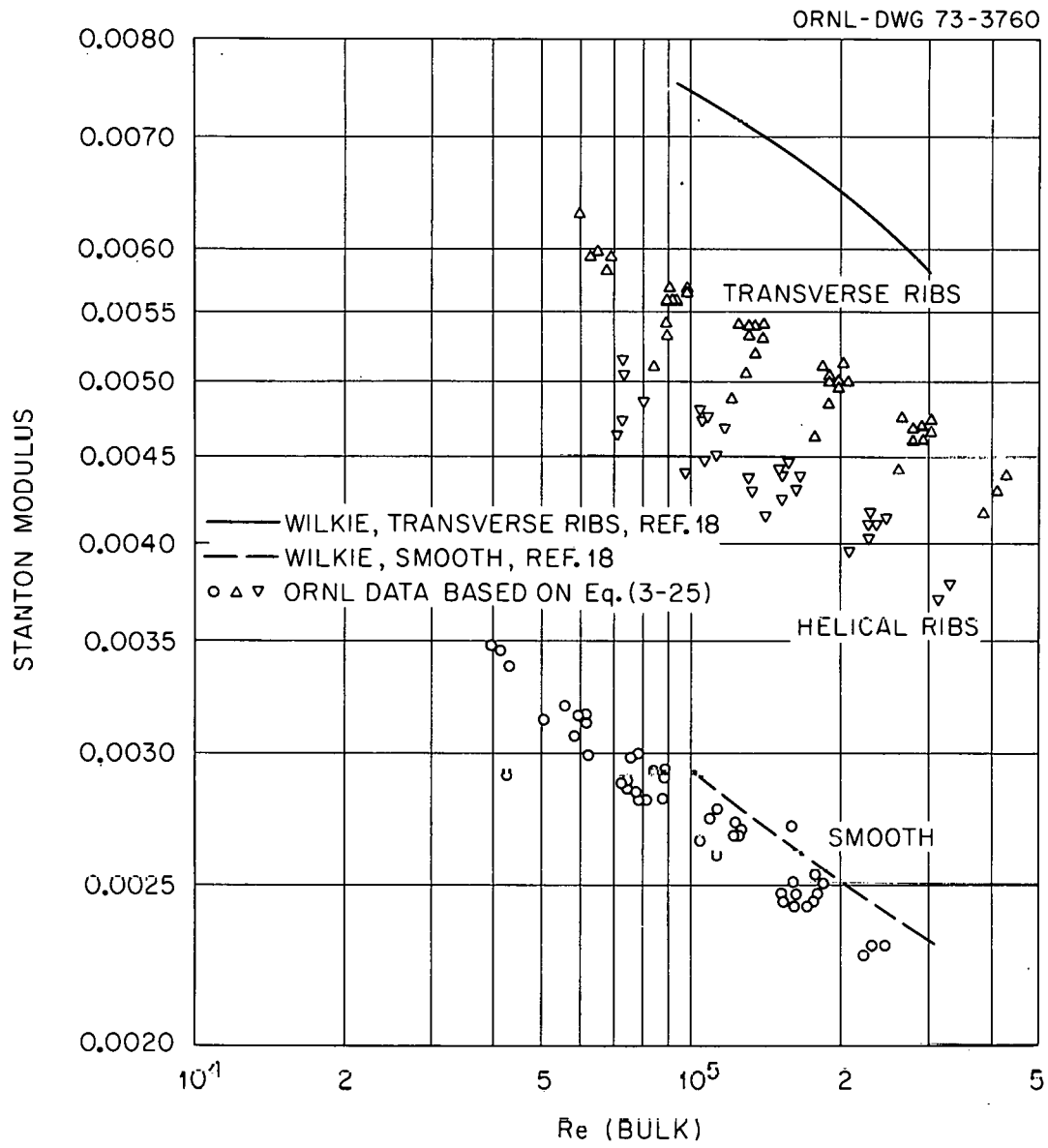
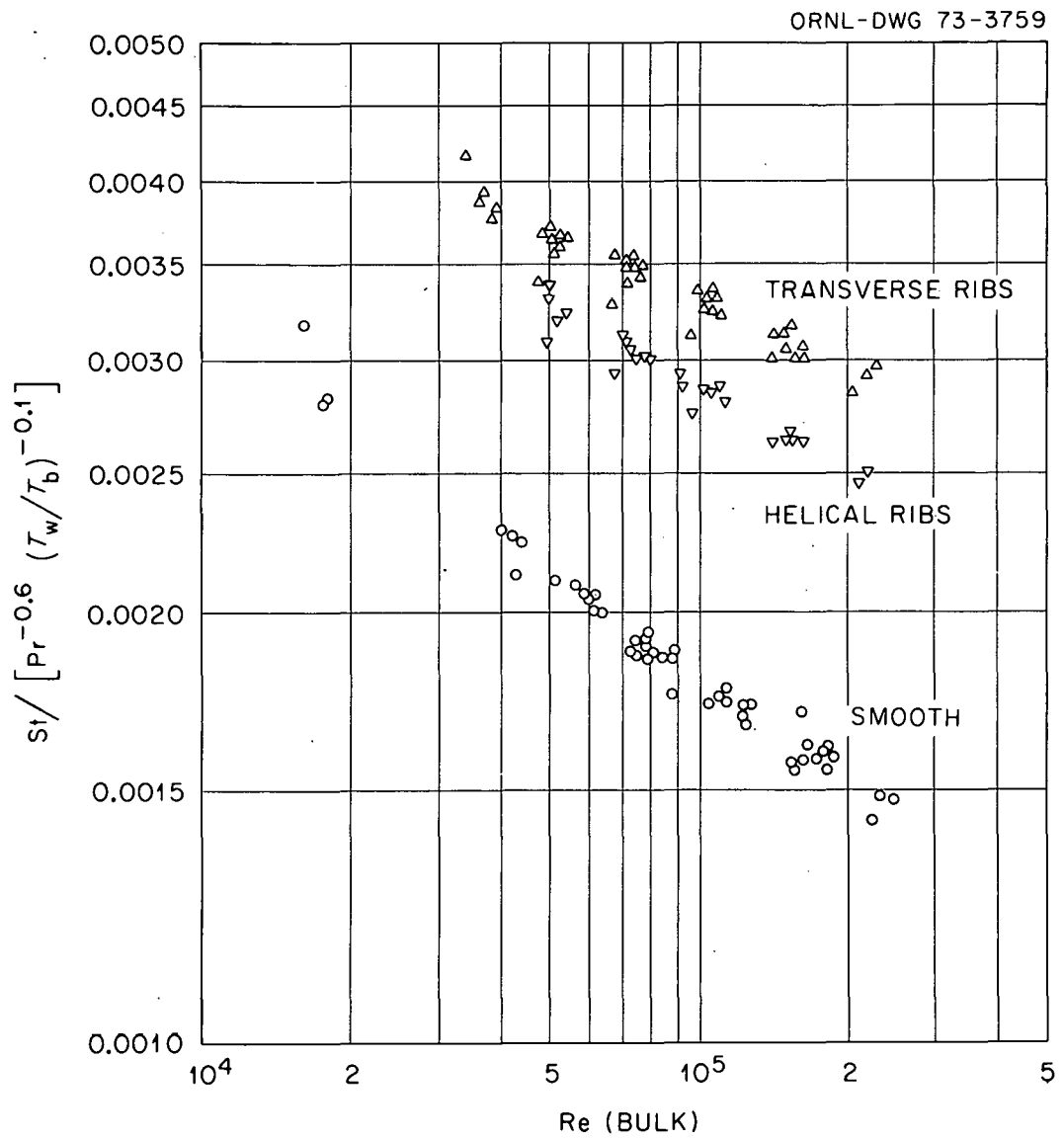


Fig. 4.4. Rod Stanton modulus.

Fig. 4.5. $\phi (St)$ - annulus.

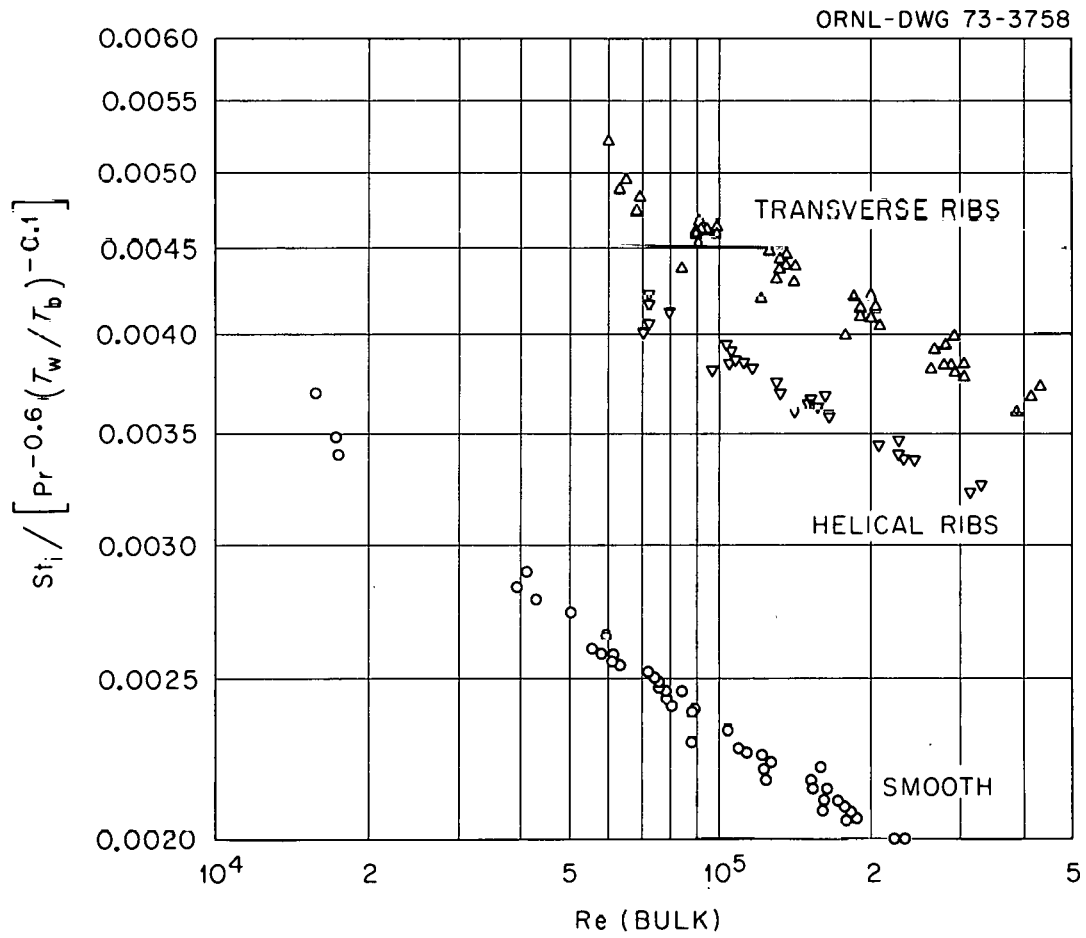


Fig. 4.6. $\phi (St_i)$ — rod, transformation Eq. (3.25).

16,000 to 450,000. Relative to a smooth surface at constant Reynolds modulus, the heat transfer coefficient of the transversely ribbed rod was from 92 to 102% better in the Reynolds modulus range from 60,000 to 300,000. The corresponding improvement for the spiral ribs ranged from 63 to 71%.

The sensitivity of the roughened rod heat transfer results to the transformation method employed is apparent in Fig. 4.7, which is based on Wilkie's^{1,2} transformation, Eq. (3.28). It will be noted that the performance of the smooth and of the spirally ribbed rods differs little from that obtained with the Hall-type¹⁰ transformation, Fig. 4.6; however, the transverse ribs, Fig. 4.7, showed $\phi(St)$ values about 10% lower than were obtained with the Hall-type transformation. Relative to a smooth surface at constant Reynolds modulus, the transversely ribbed rod showed a superiority of 68 to 86% over Reynolds modulus values between 60,000 and 300,000. The corresponding values for the spiral ribs were 54 to 67%.

4.3 Comparison with Other Results

A comparison was made with some of EIR's preliminary heat transfer and pressure drop results²¹ for photoetched spiral and transverse ribs that were tested using air at about two atmospheres. Also included were some of Wilkie's data for gaseous heat transfer with rectangular transverse ribs. The characteristics of the various surfaces are listed in Table 4.1, showing that the ratio of rib height to rod diameter for the EIR tests was about 14% smaller than for the ORNL tests; other minor discrepancies involve the ratio of rib height to width and the ratio of rod-to-shroud diameter.

The test results are summarized in Fig. 4.8 in terms of $f_i/f_{i \text{ smooth}}$ plotted against $St_i/St_{i \text{ smooth}}$ for a Re value of 100,000. The EIR values are also based on the transformation expressed in Eq. (3.25); however, their transverse rib results show slightly better heat transfer performance than the corresponding present test results. EIR's spiral rib performance, on the other hand, approaches that of the current tests. Use of Wilkie's Eq. (3.28) to transform the ORNL results reduces the Stanton

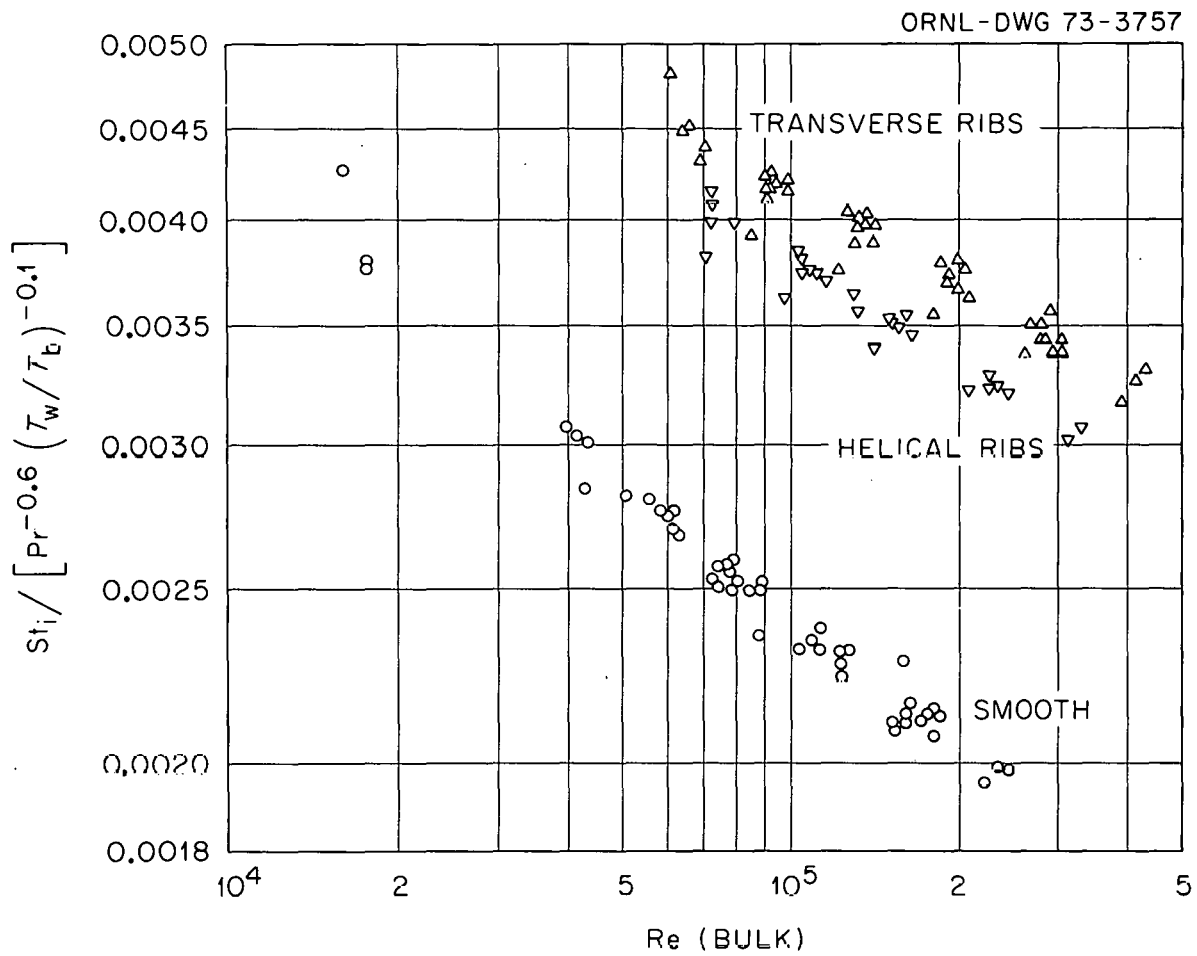


Fig. 4.7. $\phi (St_i)$ - rod, transformation Eq. (3.28).

Table 4.1. Characteristics of Rod Roughnesses

Identification	Type	Rod OD (in.)	Rib Height (in.)	Rib Width (in.)	Pitch (in.)	Rib Pitch	Rib Width	Rib Height	r_e/r_i
						Rib Height	Rib Height	OD	
EIR (Ref. 21)	Spiral ribs 34 deg helix	0.338	0.006	0.014	0.072	12.0	2.3	0.018	1.63, 2.09, and 2.56
EIR (Ref. 21)	Transverse ribs	0.338	0.006	0.018	0.072	12.0	3.0	0.018	1.63, 2.09, and 2.56
Present results	Spiral ribs	0.289	0.006	0.012	0.072	12.0	2.0	0.0208	2.07
Present results	Transverse ribs	0.288	0.006	0.012	0.072	12.0	2.0	0.0208	2.07
Wilkie (Ref. 18)	Transverse ribs	1.87				12.0			1.91

ORNL-DWG 73-3756

- SPIRAL RIBS, REF. 21
- SPIRAL RIBS, ORNL, TRANSFORMATION EQ. 3-25
- SPIRAL RIBS, ORNL, TRANSFORMATION EQ. 3-28
- TRANSVERSE RIBS, REF. 21
- ▣ TRANSVERSE RIBS, ORNL, TRANSFORMATION EQ. 3-25
- ▣ TRANSVERSE RIBS, ORNL, TRANSFORMATION EQ. 3-28
- TRANSVERSE RIBS, REF. 18

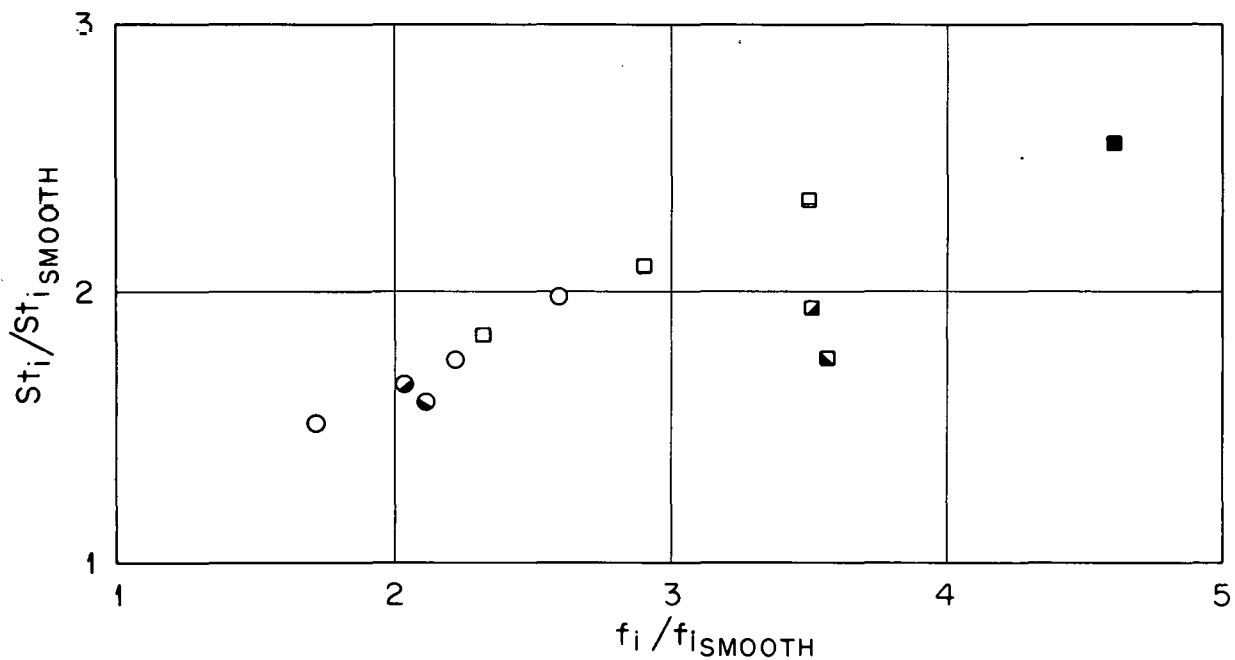


Fig. 4.8. Comparison with other data at $Re = 100,000$.

moduli for the transverse ribs by about 9% below values based on the Hall-type transformation, placing the performance of this surface about 20% below the EIR results. Wilkie's¹⁸ result for square ribs obtained using a Hall-type transformation based on actual velocity and temperature distribution measurements appears consistent with EIR's data extrapolated to higher $f_i/f_{i \text{ smooth}}$ values.

There are a number of factors that may have contributed to the discrepancies between the various experiments. The contours produced by photoetching are difficult to define precisely because the resulting ribs are not strictly rectangular and thus close matching of the EIR and ORNL results to Wilkie's data for rectangular ribs is not to be expected. Slight differences in rib shape or the surface finish of the heater rod on the flow shroud, or perhaps variances in the experimental conditions, may have contributed to the discrepancies between EIR and ORNL results. Additional uncertainties introduced by the transformations employed in data analysis are difficult to assess from the limited number of test geometries used in the present tests.

In summary, it appears that the subject tests are reasonably consistent with EIR's preliminary results; further, the tests provide useful data on the relative performance of the two roughnesses examined. In terms of the pressure drop and heat transfer parameters of Fig. 4.8, the heat transfer performance of transverse ribs is somewhat poorer than suggested by previous results.²¹

5. SURFACE EFFECTIVENESS

The performance evaluation of enhanced heat transfer surfaces should consider the heat transfer capability as well as the flow resistance of a particular design. A performance criterion suggested by Bergles²² compares the heat transfer coefficient at a given pumping power for an enhanced surface to that of a smooth surface requiring the same pumping power. In the present comparison, it was assumed that the hydraulic diameter, and the average fluid and wall temperatures were identical for the enhanced and the smooth rod. The experimental friction factors and

heat transfer coefficients were transformed to rod geometry by the methods described in Chapter 3.

The effectiveness E can be written as:

$$E = \frac{h_i}{h_{i \text{ smooth}}}, \text{ at constant pumping power} \quad (5.1)$$

If E is greater than 1.0 the surface is attractive. The pumping power requirements for the roughened rods were based on the experimentally determined friction factors. For the hypothetical smooth rod in the comparison, a flow rate was chosen that required the identical pumping power. Friction factors for the smooth rod were obtained from Eq. (4.2).

The results shown in Table 5.1 indicate that the transformation methods used in the analysis have some influence on the magnitude of E , particularly for transversely ribbed rods; the Hall-type transformation consistently resulted in an effectiveness higher than that obtained with Wilkie's transformation. On an overall basis, and bearing in mind the

Table 5.1. Surface Effectiveness

$Re \times 10^3$		60	100	200	300	400
Effectiveness spiral ribs	Transformation Eq. (3.25)	1.36	1.38	1.41	1.43	
	Transformation Eq. (3.28)	1.30	1.32	1.33	1.36	
Effectiveness transverse ribs	Transformation Eq. (3.25)	1.36	1.39	1.40	1.42	1.43
	Transformation Eq. (3.28)	1.18	1.22	1.26	1.30	1.31

uncertainties in the results, it appears that the effectiveness of the spiral ribs equals that of the transverse ribs. Compared to smooth surfaces, the enhanced surfaces showed that performance improved by 18 to

43% at constant pumping power over the range of Reynolds moduli investigated. The influence of variation in Reynolds modulus on the effectiveness is minor, generally showing a slight increase in E as Re rises from 60,000 to 400,000.

6. CONCLUSIONS

The heat transfer and pressure drop results obtained with photoetched ribbed rods showed that relative to a smooth rod, helical ribs increased the heat transfer coefficient at $Re = 100,000$, in the range from 50 to 65%, depending upon the data analysis method used. The corresponding improvements for transverse ribs ranged from 76 to 93%. The associated friction factor increases amounted to 115 to 260%, respectively, for the spiral and transversely ribbed surfaces. These conclusions are necessarily tentative because of uncertainties inherent in the methods employed to transform the annulus experimental results into a form applicable to rod surfaces. Greater confidence is held in the performance of the spiral ribs relative to that of the transverse ribs. The results indicate that in terms of an effectiveness E at constant pumping power the two surfaces perform about equally well.

Reasonably good agreement was obtained with preliminary EIR^{21} results at $Re = 100,000$ for somewhat similar photoetched rod surfaces when the same transformation was applied to both sets of data. Here the present results showed performance about equal to that cited in Ref. 21 for helical ribs and slightly poorer for the transverse ribs.

For application to multirod arrays, helical ribs may be preferred over transverse ribs, since the swirl flow induced by the former may promote interchannel mixing.

REFERENCES

1. O. H. Klepper, Heat Transfer Performance of Short Twisted Tapes, A.I.Ch.E. Symposium Series, 69(131), 87-93 (1973).
2. G. J. Kidd, Jr. and H. W. Hoffman, GCRP Semiannu. Progr. Rep., Sept. 30, 1968, ORNL-4353, pp. 129-39.
3. Letter from John B. Dee, Manager, GCFR Engineering Department, General Atomics Company, to Paul R. Kasten, Director, Gas-Cooled Reactor Program, Oak Ridge National Laboratory, Jan. 15, 1971.
4. Job Specification JS-25-245, Reactor Division, Oak Ridge National Laboratory, Aug. 23, 1971.
5. D. R. Green, R. E. Collingham, and L. H. Fischer, Infrared NDT of Electrical Fuel Pin Simulator Used in LMFR Thermal Hydraulic Tests, HEDL-TME-72-146, UC-79m (November 1972).
6. B. L. Pierce, The Thermodynamic and Transport Properties of Helium and Nitrogen, WAND-TME-1753 (1968).
7. W. M. Kays and A. L. London, Compact Heat Exchangers, 2nd Ed., p. 33, McGraw-Hill Book Company, New York, N. Y., 1964.
8. L. V. Humble, W. H. Lowdermilk, and L. G. Desmon, Measurements of Average Heat Transfer and Friction Coefficients for Subsonic Flow of Air in Smooth Tubes at High Surface and Fluid Temperatures, NACA Report 1020, Lewis Flight Propulsion Laboratory (1951).
9. W. B. Hall, "Heat Transfer in Channels Having Rough and Smooth Surfaces," J. Mech. Eng. Sci., 4(3), 287-91 (1962).
10. G. Markóczy, Konvektive Wärmeübertragung in Längsangestromten Rohr- oder Stabsbündeln, Eidg. Institut für Reaktorforschung, TM-In-430, Appendix A (April 1970).
11. B. Kjellström, Influence of Surface Roughness on Heat Transfer and Pressure Drop in Turbulent Flow, AE-RTL-821, Aktiebolaget Atomenerg, Stockholm, Sweden, 1966.
12. D. Wilkie, "Calculation of Heat Transfer and Flow Resistance of Rough and Smooth Surfaces Contained in a Single Passage," Proceedings of the Third International Heat Transfer Conference, A.I.Ch.E., Chicago, Illinois, August 1966.
13. J. G. Knudsen and D. L. Katz, Fluid Dynamics and Heat Transfer, p. 238, McGraw-Hill Book Company, New York, N. Y., 1958.

13. J. G. Knudsen and D. L. Katz, Fluid Dynamics and Heat Transfer, p. 238, McGraw-Hill Book Company, New York, 1958.
14. W. M. Kays, Convective Heat and Mass Transfer, p. 190, McGraw-Hill Book Company, New York, 1966.
15. J. G. Knudsen and D. L. Katz, Fluid Dynamics and Heat Transfer, McGraw-Hill Book Company, New York, 1958.
16. M. Hudina, Rohan Tests, Preliminary Results, Eidg. Institut für Reaktorforschung, TM-IN-463 (February 1971).
17. J. G. Knudsen and D. L. Katz, Fluid Dynamics and Heat Transfer, p. 176, McGraw-Hill Book Company, New York, 1958.
18. D. Wilkie, "Forced Convection Heat Transfer from Surfaces Roughened by Transverse Ribs," Proceedings of the Third International Heat Transfer Conference, A.I.Ch.E., Chicago, Illinois, August 1966.
19. W. M. Kays, Convective Heat and Mass Transfer, Table 9-4, McGraw-Hill Book Company, New York, 1966.
20. W. M. Kays, Convective and Mass Transfer, p. 185, McGraw-Hill Book Company, New York, 1966.
21. Letter from G. Markóczy to O. H. Klepper, January 31, 1973.
22. A. E. Bergles, A. R. Blumenkrantz, and J. Taborek, "Performance Evaluation Criteria for Enhanced Heat Transfer Surfaces," Paper No. 9, AIChE-ASME Thirteenth National Heat Transfer Conference, Denver, Colorado, August 1972.

LIST OF SYMBOLS

A	Flow area normal to tube axis
C	Constant
C_p	Specific heat
D_h	Flow channel hydraulic diameter
E	Effectiveness, $h_i/h_{i \text{ smooth}}$ at constant pumping power
f	Blasius friction factor
f_s	Friction factor for smooth annulus
g_c	Proportionality constant relating force to the product of mass and acceleration
G	Mass velocity
h	Heat transfer coefficient
k	Thermal conductivity
K	Effective gas thermal conductivity
p	Perimeter
P	Pressure
Pr	Prandtl modulus, $\frac{C_p \mu}{k}$
\dot{q}_l	Heat flux
Q_e	Total electrical heat generation rate
Q_g	Total rate of heat transfer to gas
Q_l	Total rate of heat transfer to insulation
r	Radius
Re	Reynolds modulus, $\frac{\rho V D}{\mu}$
Re_I	Modified Reynolds modulus based on bulk velocity and properties evaluated at T_I , $\rho_I \overline{VD}/\mu_I$
St	Local Stanton modulus, $\frac{h}{C_p G}$
T	Temperature, °R
T_b	Bulk gas temperature, °R
T_w	Rod surface temperature, °R
T_I	Characteristic fluid temperature, $0.05 (T_w - T_b) + T_b$, °R
V	Velocity
\bar{V}	Average velocity
W	Mass rate of flow
X	Axial position along length of annulus

Greek Symbols

δ	Thickness of laminar sublayer
ΔH	Enthalpy rise
ΔP	Pressure drop
ΔT	Temperature drop
ϵ_H	Turbulent diffusivity of heat
ν	Kinematic viscosity
μ	Fluid viscosity
μ_I	Fluid viscosity based on T_I
ρ	Bulk density based on T_b
ρ_I	Bulk density based on T_I
τ	Wall shear stress
$\phi(St)$	Nondimensional function of local Stanton modulus

Subscripts

1	Entrance
2	Exit
i	Inner flow channel
e	Outer flow channel
o	Zero shear surface
s	Smooth surface

THIS PAGE
WAS INTENTIONALLY
LEFT BLANK

Appendix A

Digital Computer Program

THIS PAGE
WAS INTENTIONALLY
LEFT BLANK

```

**PTN,L,E,M,G.
C PROGRAM GASHT2 FOR REDUCING HEAT TRANSFER AND PRESSURE DROP DATA
C FROM GASEOUS FLOW TESTS IN ANNULAR GEOMETRY
  DIMENSION YB(10),Y(10),X(10),TW(10),TWB(10),TT(10),
  1TTB(10),XD(10),XPL(10),F(10),DH(10),PB(10),HCCI(10),EPT(10),
  2SN(100),DU(100),H(10),TGB(10),RHOGAS(10),SPECHT(10),COD(10),
  3VSC(10),THS(10),HRAC(10),HTC(10),ST(10),USS(10),FE(10),TRAT(10),
  4PR(10),FEEST(10),FEEUSS(10),TGTAP(10),AE(10),APET(10),TEFF(10),
  5RHOEFF(10),VSCEPF(10),PPA(10),REFA(10),TSB(10),HFLUX(10),PPH(10),
  6DZERO(10),STH(10),REFZ(10),REZ(10),DEZ(10),PFS(10),PPAA(50),
  7REFAA(50),PPHA(50),REFZA(50),PEESTA(50),REA(50),FEESTH(50),
  8FSTHA(50),REZA(50),FPSA(50)
C FUNCTION STATEMENT FOR THERMAL CONDUCTIVITY
  TCO(A) = 8.5 + .004167 * A
  K = 0
  READ 8, (SN(I),DU(I),I=1,25)
  5 READ(50,8,END = 500) (SN(I),DU(I),I= 26,60)
  8 FORMAT(5(I3,F10.0,2X))
  K = K + 1
C HEATER DIA. = OD, INCHES
  CE = DU(19)
C SHROUD ID = SD, INCHES
  SE = DU(20)
C OUTER SHEATH THICKNESS = CT, INCHES
  CT = DU(21)
  DO 200 I = 1,10
  200 X(I) = DU(I)
  DO 201 I = 2,7
  201 Y(I) = DU(I + 9)
  DO 202 I = 1,8
  TW(I) = DU(I + 26)
  202 TT(I) = DU(I + 34)
  DO 204 I = 1,4
  P(I) = DU(I + 42)
  204 DH(I) = DU(I + 55)
CALC SEGMENT PARAMETERS
C YB = DISTANCE TO SEGMENT MID LENGTH
  YB(1) = (Y(8) + X(2)) / 2.
  DO 10 I = 2,6
  10 YB(I) = (Y(I + 1) + Y(I)) / 2.
  YB(7) = (X(9) + Y(7)) / 2.
  YB(8) = (X(10) + X(9)) / 2.
CALC REQ SEGMENT LENGTHS XD, IN.
  XD(1) = Y(2) - X(2)
  DO 50 I = 2,6
  50 XD(I) = Y(I+1) - Y(I)
  XD(7) = X(9) - Y(7)
CALC PRESS DROP SEGMENT LENGTHS
  XPL(1) = X(5) - X(3)
  XPL(2) = X(6) - X(5)
  XPL(3) = X(8) - X(6)
C TWB = SEGMENT TUBE OD TEMP DEG. F
  TGRAD = (TW(5) + TW(6) - TW(3) - TW(4)) / (2. * (X(7) - X(4)))
  TWB(1) = TW(2)
  DO 20 I = 2,8
  20 TWB(I) = (TW(3) + TW(4)) / 2. + TGRAD * (YB(I) - X(4))
C TTB = AVG THERMOCOUPLE TEMP FOR SEGMENT, DEG F
  TTB(3) = (TT(1) + TT(2) + TT(3) + TT(4)) / 4.
  TTB(4) = (TT(3) + TT(4) + TT(5) + TT(6)) / 4.
  TTB(5) = (TT(5) + TT(6) + TT(7) + TT(8)) / 4.
CALCULATE TAP AND SEGMENT PRESSURES, PSIG
C ASSUME HG AT MANOMETER REFERENCE TEMP. = 68 DEG F
  SFGRHG = 13.546
  DO 30 I = 2,4
  30 P(I) = P(I - 1) - SFGRHG * 62.44 * DH(I - 1) / 1728.
C PB = AVG SEGMENT PRESSURE PSIG
  PB(2) = P(1) + (P(3) - P(4)) * (Y(3) - YB(2)) / (Y(6) - Y(5))
  PB(1) = PB(2) + (F(3) - P(4)) * (Y(3) - YB(2)) / (Y(6) - Y(5))
  PB(3) = P(1) - (P(1) - P(2)) * (YB(3) - Y(3)) / (Y(4) - Y(3))

```

```

PB(4) = P(2) - (P(2) - P(3)) * (YB(4) - Y(4)) / (Y(5) - Y(4))
PB(5) = P(3) - (P(3) - P(4)) * (YB(5) - Y(5)) / (Y(6) - Y(5))
PB(6) = P(4) - (P(3) - P(4)) * (YB(6) - Y(6)) / (Y(6) - Y(5))
PB(7) = P(4) - (P(3) - P(4)) * (YB(7) - Y(6)) / (Y(6) - Y(5))
C PX2 = PRESS AT X(2)
  PX2 = P(1) + (P(3) - P(4)) * (Y(3) - X(2)) / (Y(6) - Y(5))
C PX9 = PRESS AT X(9)
  PX9 = P(4) - (P(3) - P(4)) * (X(9) - Y(6)) / (Y(6) - Y(5))
CALCULATE FLOWRATE LBS/SEC = FOW
  PORF2 = DU(47)
  DHORF = DU(48)
C ORIFICE DP = DPORF IN PSI
  DPORF = DHORF * SFGRHG * 62.44 / 1728.
  PORF1 = PORF2 + DFORF
  TGR = DU(49)
  CALL TP(TGR,PORF1,SS,V,GA,VV,WW,XX,ZZ,QQ)
  RHUORF = 1. / V
C SPECIFIC HEAT RATIO = SPHRAT
  SPHRAT = GA
C DORG = ORIFICE DIA. (IN)
C DISCHARGE COEFFT / SQRT(1.- BETA**4) = QUAY
  DORF = DU(50)
  QUAY = DU(51)
  X1 = (PORF1 - PORF2) / (PORF1 + 14.7)
C PDA = PIPE DIA. (IN)
  PDA = DU(18)
  BETA = DORF / PDA
  Y1 = 1. - (.41 + .35 * BETA**4.) * (X1 / SPHRAT)
C FLOW = FOW
  FOW = .525 * QUAY * Y1 * DORF * DORF * SQRT(EHCORF * DFORF)
C FLOW AREA = FAR, SQ FT
  FAR = 3.1415 * (SD * SD - CD * OD) / (4. * 144.)
C GEE = MASS FLOWRATE LBS. / SQ. FT. SEC.
  GFE = FOW / FAR
  SQG = GEE * GFE
CALC HEAT LOSS FROM SHRCOL FOR SEGMENTS 1 THRU 7= HCONC,BTU / HR
C TV1 = PRESSURE SHELL TEMP. DEG F
  TV1 = DU(26)
  DO 40 I = 1,7
    40 HCOD(I) = .014 * XD(I) * (TWB(I) - TV1)
CALCULATE HEATER INPUT FOR EACH SEGMENT = EPT,BTU / HR
C EV = HEATER VOLTAGE
CURR = AMPERAGE
  EV = DU(53)
  CURR = DU(54)
  DO 60 I = 2,6
    60 EPT(I) = 3.4122 * EV * CURR * XD(I) / (Y(7) - Y(2))
    EPT(7) = 0.
CALC GAS TEMP FOR EACH SEGMENT.FIRST GET ENTHALPY AT X(2) = H
C ASSUME GAS TEMP AT X(2) = TW(2)
  TGAS2 = TW(2)
  CALL TP(TGAS2,PX2,HGAS,VV,UU,SS,TTT,RR,YY,ZZ)
  H(1) = HGAS
  H(2) = H(1) + (EPT(2) - HCOD(2)) / (2. * FOW * 3600.)
  DO 70 I = 3,7
    70 H(I) = H(I-1) + (EPT(I) + EPT(I-1) - HCOD(I) - HCOD(I-1)) / (2. * FOW * 3600.)
  DO 75 I = 2,7
    EGAS = PB(I)
    HGAS = H(I)
    CALL HP(HGAS,PGAS,AA,TTT2,V,CC,DD,EE,GG,HH,UU,VV,XX)
    TGB(I) = TTT2
C TGR = SEGMENT BULK GAS TEMP
  RHOGAS(I) = 1. / V
  SPECHT(I) = DDD
  CCD(I) = GGG
  75 VSC(I) = HH
CRHOGAS = LBS/CU FT SPECHT = BTU/DEG F LB COD = BTU/PT SEC DEG F
C VSC = LBS / PT SEC

```

```

CALC HEAT BALANCE BETWEEN X(2) AND X(9).GET ENTHALPY AT X(9)
CALL TP(TW(7),PX9,HGAS,VV,UU,SS,TTT,RR,YY,ZZ)
H(8) = HGAS
AEGAS = ( H(8) - H(1) ) * POW * 3600.
C AEGAS = GAS ENERGY GAIN BTU/ HR
C ENERGY LOSS FROM TUBE BETWEEN X(2) AND X(9) = SHCOD
SHCOD = 0.
DO 80 I= 1,7
80 SHCOD = HCOD(I) + SHCOD
C ERROR = PERCENT ERROR IN HEAT BALANCE
EPUT = 3.4122 * EV * CURR
ERROR = (EPUT - SHCOD - AEGAS) * 100. / EPUT
CALC TEMP DIFF BFTWWFEN HEATER SURFACE AND TC ASSUMING JUNCT AT TC CL
C TD = DIA AT HEATER TC CIRCLE,IN
TD = OD-2.*( .01 + CT)
DO 100 I = 3,5
TSS = TTB(I)
100 THS(I)=TTB(I)-12.*(EPT(I)*ALOG(OD/TD))/(TCO(TSS)*3.141*XD(I)*2.)
C THS = HEATER SURFACE TEMP DEG F
CALC. ROD SEGMENT RADIANT HEAT TRANSFER FOR GRAY ENCLCSURE EMM. =.5
CO 90 I= 3,5
CO90 = ((THS(I) + 460.)/100. )**4.-((TWE(I) + 460.)/100. )**4.
90 HRAD(I) = .1415 * CD * XD(I) *.4 *.171 * CO90 /144.
C EQUIV DIA = DEQ
DEQ = SD - OD
CALC SEGMENT PARAMETERS HTC = HEAT TRANSFER COEFF BTU/HR SQ FT DEG F
DO 110 I = 3,5
HFLUX(I)=( EPT(I) -HRAD(I) ) * 144./ ( 3.1415 *OD*XD(I))
HTC(I) = HFLUX(I) / ( THS(I) - TGB(I) )
C NUSSELT= USS,ST=STANTON,RE=REYNOLDS,TRAT=TW/TB,PR=PFANDTL
ST(I) = HTC(I) / ( SPECHT(I) * GEE * 360C.)
USS(I) = HTC(I) * DEQ / ( 43200.* COD(I))
RE(I) = DEQ * GEE / ( VSC(I) * 12.)
TRAT(I) = ( THS(I) + 460. ) / ( TGB(I) + 460. )
PR(I) = SPECHT(I) * VSC(I) / COD(I)
CO110 = .1
FEEST(I) = ST(I) * PR(I) **.6 *TRAT(I)**CC110
FEEST(I) = ST(I)
CO111 = .5
110 FEPUSS(I) = USS(I) * TRAT(I)**CO111 / ( PR(I) **.4)
CALC TEMPS AND PRESS AT TAPS AND AVERAGED CVFF TAP SEGMENTS
C TGTAP = TEMP AT TAP
DO 120 I = 1,4
TGTAP(1) =TGB(2)+(TGB(3)-TGB(2))*(X(3)-YE(2))/(YB(3) - YB(2))
TGTAP(2) = TGB(3)+(TGB(4)-TGB(3))*(X(5)-YB(3))/(YB(4)-YB(3))
TGTAP(3) =TGB(4)+(TGB(5)-TGB(4))*(X(6)-YE(4))/(YB(5)-YB(4))
120 TGTAP(4)=TGB(5)+(TGB(6)-TGB(5))*(X(8)-YE(5))/(YB(6)-YB(5))
NORUN = DD(55)
PRINT 125,NORUN
125 FORMAT(1H1,30X,'PRESSURE DROP DATA RUN ',I3)
PRINT 127
127 FORMAT(1H0,'SEGMENT NO BB TEPF FHOEPF AP APNET PFA
1 REPA FFH DZERO RE ROC')
CALC NET PRESSURE DROP ACCOUNTING FOR ACCELERATION
DO 130 I= 1,3
AP(I) = P(I) - P(I+1)
CALL TP(TGTAP(I),F(I),CCC,V,DDD,FEE,GGG,UUU,VVV,WWW)
GASD1 = 1. / V
CALL TP(TGTAP(I+1),P(I+1),CCC,V,DDD,FEE,GGG,UUU,VVV,WWW)
GASD2 = 1. / V
CO130 = 1. / GASD1 -1. / GASD2
CO131 = SQG / ( 32.2* 144.)
130 APET(I) = AP(I) + CC130 * CO131
C. DECREASE AP1 TO ACCOUNT FOR .0006 IN, INCREASE AT C1
PAR1 = 3.1415 * (.6006 * .6006 - CD * OE) / (4. * 144.)
CO132 = 1. - (PAR1 / FAR)**2.
CORR1 = CO131 * CO132 / (RHOGAS(3) * 2.)
APET(1) = APET(1) + CORR1

```



```

C INCREASE AP3 TO ACCOUNT FOR .004 IN. INCREASE AT D4
PAR4 = 3.1415 * (.604 * .604 - OD * OD) / (4. * 144.)
CO133 = (PAR4 / FAF)**2. - 1.
CORR3 = CO133 * CO131 / (RHOGAS(5) * 2.)
APPT(3) = APPT(1) + CORR3
C PFA = PF WITH DENS AND VISC BASED ON EFFECTIVE TIME BUT ACTUAL VELOCITY
BB = .05
DO 150 I = 3,5
TEFF(I) = BB * ( THS(I) - TGB(I) ) + TGB(I)
CALL TP(TEFF(I), PE(I), CC, V, DD, EE, GG, UU, VIG, VV)
RHOEFF(I) = 1. / V
VSCEFF(I) = VIG
CO150 = 298. * DEQ * RHOGAS(I) * RHOGAS(I) * 32.2
CO151 = XPL(I - 2) * SQG * RHOEFF(I)
PFA(I) = CO150 * APET(I - 2) / CO151
CO152 = GEE * DEQ / 12.
CO153 = RHOEFF(I) / RHOGAS(I)
REFA(I) = CO152 * CO153 / VSCEFF(I)
C APPLY HALL TRANSFORM TO F.P.
C UU = CHANNEL PERIMETER
UU = 3.1415 * (OD + SD)
C UU2 = PERIMETER OUTER CHANNEL
UU2 = 3.1415 * SD
UUX = UU2 / UU
C FFS = PF CORRELATED FOR SMOOTH CHANNEL
FFS(I) = .118 * (REFA(I)**(-.155) )
CO160 = 1. - ( UUX * (PFA(I) / FFS(I) ) **(-.8) )
PPH(I) = PFA(I) * CO160 / ( 1. - UUX )
C CALC. ZERO SHEAR DIAMETER = DZERO
CO161 = (SD**2. - CD**2.) * SD * (PFA(I) / FFS(I) ) **(-.8)
DZERO(I) = (SD**2. - CO161 / (OD + SD) ) **.5
CALC RE BASED ON DZERO = REFZ, DEZ = D, HYDR. INNER CHANNEL
DEZ(I) = ( DZERO(I)**2. - OD**2. ) / OD
REFZ(I) = REFA(I) * DEZ(I) / DEQ
PRINT 160, I, EE, TEFF(I), RHOEFF(I), AP(I - 2), APET(I - 2), PFA(I),
1 REFA(I), PPH(I), DZERO(I), REFZ(I)
160 FORMAT(1H0,5X,I5,4X,F7.4,2X,F5.0,3(2X,F5.3),X,F6.5,2X,P8.0,2X,
1F6.5,1X,P6.1,1X,P6.5)
150 CONTINUE
DO 155 I=3,5
C APPLY HALL TRANSFORM TO STANTON NO.
CO170 = ( ( SD/OD)**2. - 1. )**2.
CO171 = ( ( SD/OD )**4. ) * (4. * ALOG(SD/CD) - 3. )
CO172 = 4. * ( SD/CD )**2. - 1.
PEEONE = CO170 / ( CO171 + CO172 )
CO180 = ( ( DZERO(I) / OD )**2. - 1. )**2.
CO181 = ( (DZERO(I)/CD)**4. ) * (4. * ALOG(DZERO(I) / OD) - 3. )
CO182 = 4. * (DZERO(I) / OD )**2. - 1.
PEETWO = CO180 / ( CO181 + CO182 )
CO185 = (THS(I) - TGE(I)) * COD(I) * PPH(I) * GEE * 3600. / (8. * VSC(I) *
1 HFLOX(I) )
STH(I) = CO185 / ( (CO185 - 1.) * PEEONE / PEETWO + 1. ) * ST(I)
FEESTH(I) = STH(I) * PR(I) **.6 * TRAT(I) ** CO110
FEESTH(I) = STH(I)
CALC RE BASED ON DZERO = REZ
155 REZ(I) = RE(I) * DEZ(I) / DEQ
PRINT 170, NORRN
170 FORMAT(1H0,30X,'HEAT TRANSFER DATA RUN ',I3)
PRINT 172
172 FORMAT(1H0,'SEGMENT NO GAS PRESS GAS TEMP GAS LENS VISCOCITY
1SURF TEMP SHROUD TEMP IG/TE')
PRINT 173, (I, PB(I), TGB(I), RHOGAS(I), VSC(I), THS(I), TWB(I), TRAT(I),
1I=3,5 )
173 FORMAT(1H0,4X,I2,8X,F7.2,5X,P6.1,4X,P6.4,3X,P9.8, 3X,P6.1,4X,P6.1,
1 6X,F5.3)
PRINT 174

```

```

174  FORMAT(1H0,'SEGMENT NO HEAT FLUX NUSSEIT STANTON RE EQUIV NUSS
      1LT FUNCTION ST FUNCTION          H      HALL ST RE ROD FEESTH')
      PRINT 175,(I,HFLUX(I),USS(I),ST(I),RE(I),FEEUSS(I),FEEST(I),HTC(I
      1),STH(I),REZ(I),FEESTH(I),I=3,5)
175  FORMAT(1H0,4X,I2,7X,P7.0,3X,P6.1,4X,P7.5,X,P8.0,3X,P7.1, 6X,P9.7,2
      1X,P7.0,4X,P7.5,3X,P8.0,2X,P8.6)
      CALL POINT(H      ,EPT,HCOD,TGTAP,P,Y,HFLUX,TT,XD,GEE,DEQ,NORUN,POW,
      1 OD,TD)
      PRINT 176
176  FORMAT(1H1,30X,'INPUT DATA')
      PRINT 177
177  FORMAT(1H0,' I      X(I) Y(IN) TW(DEG F) TT(DEG F) P(PSIG) DH(IN
      1HG ) ')
      PRINT 178 , (I,X(I),Y(I),TW(I),TT(I),P(I),DH(I),I=1,10)
178  FORMAT(1H0,2X,I2,4X,P5.3,X,P6.3,2X,P6.1,3X,P6.1,4X,P5.0,4X,P6.3)
      PRINT 179,OD,SD,CT,TV1,PORF2,DHORF,TGF,ECRF,QUAY,PDA,EV,CURR,EPUT
      1,HERROR,POW
179  FORMAT(1H0,'OD = ',P6.4,' SD = ',P6.4,' CT = ',P6.4,' TV1 = ',
      1P6.1,' PORF = ',P6.0,' DHORF = ',P7.4,' TGF = ',P6.0,' DHORF =
      2 ',P6.3,' QUAY = ',P6.4,' PDA = ',P6.3,' EV = ',P6.2,' CURR =
      3 ',P6.2,' EPUT = ',P5.1,'/','HERROR = ',P6.3,' PLCH = ',P6.4)
      CALL BIGAR(PFA,REFA,PFH,REF2,FEEST,RE,FPS,FEESTE,REZ,K,PFAA,REFAA
      1,PFHA,REFZA,FEESTA,REA,FFSA,PSTHA,REZA)
      GO TO 5
500  CONTINUE
      CALL PLPPA
C   FOR PLOTTING ANNULUS FF
      CALL QQQCPA(10,-1)
      CALL LINPLT(REFAA(1),PFAA(1),K,+4.0,-1)
      CALL PLPPH
C   FOR PLOTTING ROD FF
      CALL QQQCPA(10,-1)
      CALL LINPLT(REFZA(1),PFHA(1),K,+4,-1)
      CALL LINPLT(REFZA(1),PFSA(1),K,+1,-1)
      CALL PLSTA
C   FOR PLOTTING ANNULUS STANTON FUNCTION
      CALL QQQCPA(10,-1)
      CALL LINPLT(REA(1),FEESTA(1),K,+4.0,-1)
      CALL PLSTAR
C   FOR PLOTTING ROD STANTON FUNCTION
      CALL QQQCPA(10,-1)
      CALL LINPLT(REZA(1),PSTHA(1),K,+4.0,-1)
      CALL ADVANS
      END

```

```

      SUBROUTINE POINT(H      ,EPT,HCOD,TGTAP,P,Y,HFLUX,TT,XD,GEE,DEQ,
      1 NORUN,POW,OD,TD)
      DIMENSION EPT(10),HCOD(10),TGTAP(10),P(10),Y(10),TGY(10),
      1 ROGASY(10),COBY(10),VSCY(10),HFLUX(10),TTY(10),THSY(10),XD(10),
      2 HTCY(10),STY(10),SPCHTY(10),USSY(10),REY(10),TRATY(10),PBY(10),
      3 FEESTY(10),FEEUSSY(10),HY(10),PY(10),TT(10),H(10)
C   SUBROUTINE TO CALC. HEAT TRANSP. PERF. AT Y(3) THRU Y(7)
C   FIRST GET LOCAL GAS TEMPS. = TGY
      TCO(A) = 8.5 + .004167 * A
      HY(2) = H(1)
      DO 10 I = 3,7
10  HY(I) = HY(I-1) + (EPT(I-1) - HCOD(I-1)) / (POW * 3600.)
C   ASSUME PRESS AT Y(3) = P(1) = PY(3), ETC.
      DO 20 I = 3,6
20  PY(I) = P(I-2)

```

```

      CALL HP(HY(I),PY(I),AA,TTT,V,CC,DD,EE,GGG,HH,UU,VV,XX)
      TGY(I) = TTT
      ROGASY(I) = 1. / V
      SPCHTY(I) = DE
      CODY(I) = GGG
20  VSCY(I) = HH
C   ROGASY = LBS/CU FT,SECHTY = BTU/DEG F LE,CCEY = BTU/PT SEC DEG F
C   VSCY = LBS / PT SEC,ASSUME HEAT FLUX = SEGMENT HEAT FLUX
      HFLUX(6) = HFLUX(5)
C   CALC. SURF. TEMP. AT THERMOCOUPLE LOCATIONS
      TTY(3) = ( TT(1) + TT(2) ) / 2.
      TTY(4) = ( TT(3) + TT(4) ) / 2.
      TTY(5) = ( TT(5) + TT(6) ) / 2.
      TTY(6) = ( TT(7) + TT(8) ) / 2.
C   CALC. DELTA T ACROSS OUTER SHEATH ,HEATER SURF. TEMP. = THSY
      DO 30 I = 3,6
      TSS = TTY(I)
      THSY(I) = TTY(I) - 12. * (EPT(I) * ALOG(CD/TD)) / (TCO(TSS) * 3.141 * ID(I) * 2.
1 )
C   CALC HEAT TRANSF. PARAMETERS
      HTCY(I) = HFLUX(I) / ( THSY(I) - TGY(I) )
      STY(I) = HTCY(I) / ( SPCHTY(I) * GEE * 3600.)
      USSY(I) = HTCY(I) * DEQ / ( 43200. * CODY(I) )
      REY(I) = DEQ * GFE / ( VSCY(I) * 12. )
      TRATY(I) = (THSY(I) + 460. ) / ( TGY(I) + 460.)
      PRY(I) = SPCHTY(I) * VSCY(I) / CODY(I)
      CO30 = 0
      FEESTY(I) = STY(I) * PRY(I) **.6 * TRATY(I) **.6 * CO30
      CO31 = .5
30  FEENSY(I) = USSY(I) * TRATY(I) **.6 * CO31 / ( PRY(I) **.4)
      PRINT 35, NORUN
35  FORMAT(1H0,30X,'PCINT HEAT TRANSFER DATA RUN ',13)
      PRINT 37
37  FORMAT(1H0,'SEGMENT NO  GAS PRESS  GAS TEMP  GAS DENS  VISCOCITY
1 SURF TEMP  TG/TE')
      PRINT 38, (I,PY(I),TGY(I),ROGASY(I),VSCY(I),THSY(I),TRATY(I),I=3,6)
38  FORMAT(1H0,4X,I2,UX,F7.2,5X,F6.1,4X,F6.4,3X,F9.8, 3X,F6.1,6X,F5.3)
      PRINT 40
40  FORMAT(1H0,'      Y      HEAT FLUX  NUSSEIT  STANTON  RE EQUIV  NUSS
1LT FUNCTION  STANTON FUNCTION  R')
      PRINT 41, (I,HFLUX(I),USSY(I),STY(I),REY(I),FEENSY(I),FEESTY(I),
1 HTCY(I),I = 3,6)
41  FORMAT(1H0,4X,I2,7X,F7.0,3X,F6.1,4X,F7.5,X,F8.0,3X,F7.1,13X,F9.7,5
1X,F7.0)
      RETURN
      END POINT

```

```

      SUBROUTINE TP (T,P,H,V,GA,CP,SV,C,VIG,ICE)
C   CONVERT TEMPERATURE FROM DEGREES F TO DEGREES RANKIN.
      TT=T+460.
C   CONVERT GAUGE PRESSURE TO ABSOLUTE PRESSURE (ALL IN LB./SQ.IN.).
      PP=P+14.7
C   CALL TABTP (TT,PP,H,V,GA,CP,SV,C,VIG,ICE)
C   CONVERT SPECIFIC VOLUME FROM CU.IN./LB. TO CU.FT./LB.
      V=V/1728.
C   CONVERT THERMAL CONDUCTIVITY FROM BTU/IN.SEC.DEGREE R TO BTU/FT.-
C   DEGREE F.
      C=C*12.
C   CONVERT ABSOLUTE VISCOSITY FROM LB/IN.SEC. TO LB./PT.SEC.
      VIG=VIG*12.
      RETURN
      END

```

```

SUBROUTINE HP (H,P,Q,T,V,GA,CP,SV,C,VIG,VIL,VG,VI)
C  CCNVERT GAGE PRESSURE TO ABSOLUTE PRESSURE (LB./SQ.IN.).
  PP=P+14.7
  CALL TABHP (H,PP,Q,T,V,GA,CP,SV,C,VIG,VIL,VG,VI)
C  CCNVERT TEMPERATURE FROM DEGREES R TO DEGREES F.
  T=T-460.
C  CONVERT SPECIFIC VOLUME FROM CU.IN./LB. TO. CU.FT./LB.
  V=V/1728.
C  CONVERT THERMAL CONDUCTIVITY FROM BTU/IN.SEC.DEGREE R TO BTU/FT.-
C  SEC.DEGREE F.
  C=C*12.
C  CONVERT ABSOLUTE VISCOSITY FROM LB/IN.SEC. TO LB/FT.SEC.
  VIG=VIG*12.
  RETURN
END

```

C	SUBROUTINE TABTP(TT,PP,H,V,GA,CP,SV,C,VIG,ICE)	TABTP 10
	NITROGEN	TABTP 20
	DIMENSION W(11)	TABTP 30
	DATA KO,K/0,1/	TABTP 40
	T=TT	TABTP 50
	P=PP	TABTP 60
	GO TO (1,2),K	TABTP 70
1	K=2	TABTP 80
	WRITE (6,1001)	TABTP 90
1001	FORMAT(1H0,10(10H*****)/42H NITROGEN FLUID PROPERTIES *WANL-TTABT 100	
	1ME-1753*)	TABT 101
2	IFLAG=0	TABT 110
	IF(T.GE.120.) GO TO 3	TABT 120
	IFLAG=1	TABT 130
	T=120.	TABT 140
3	IF(T.LE.4500.) GO TO 4	TABT 150
	IFLAG=1	TABT 160
4	IF(P.GT.0.0) GO TO 5	TABT 170
	IFLAG=1	TABT 180
	P=.1	TABT 190
5	IF(P.LE.2500.) GO TO 6	TABT 200
	IFLAG=1	TABT 210
6	IF(IFLAG.EQ.0) GO TO 7	TABT 220
1002	FORMAT(25HCIND VAR. OUT OF RANGE X=P10.1,10H PRESSURE=P10.1)	TABT 230
	IF(KO.GT.20) GO TO 7	TABT 240
	WRITE (6,1002) T,P	TABT 250
	KC=KC+1	TABT 260
7	IF(T.GE.910.) GO TO 8	TABT 270
	CALL NITRO(T,P,W(2),W(1),W(5),W(3),W(4))	TABT 280
	IF(T.LE.890.) GO TO 10	TABT 290
8	CALL NIT900(T,P,W(6))	TABT 300
	IF(T.GE.910.) GO TO 11	TABT 310
	X=(T-890.)/20.	TABT 320
	X1=1.-X	TABT 330
	DO 9 I=1,5	TABT 340
9	W(I)=X1*W(I)+X*W(I+5)	TABT 350
10	IS=1	TABT 360
	GO TO 12	TABT 370
11	IS=6	TABT 380
12	H=W(IS)	TABT 390
	V=W(IS+1)	TABT 400
	GA=W(IS+2)	TABT 410
	CP=W(IS+3)	TABT 420
	SV=W(IS+4)	TABT 430

	T=T/1.8	TABT 440
	RHO=988.024/W (IS+1)	TABT 450
	TH=T/126.26	TABT 460
	IF (TR.GT.1.) GO TO 13	TABT 470
	VIS=8.65E-5*(TR)**0.979	TABT 480
	GO TO 15	TABT 490
13	IF (TR.LT.3.5) GO TO 14	TABT 500
	VIS=10.3454E-5*(TR)**0.659	TABT 510
	GO TO 15	TABT 520
14	VIS=10.E-5* (-.77704535E-1+T*(.86124288E-2+T*(-.10126169E-4+T*(.70	TABT 530
	1740430E-8))))	TABT 531
15	X=RHO*.028016	TABT 540
	XX=(X/.7)**3	TABT 550
	BRHO=37.8978+27.2E64*(XX**2-SQRT(XX))-66.8138*EXP(-58.75*XX)	TABT 560
	ARHO=EXP(3.4664+AICG(X)+2.0557*XX**1.5-6.E-6*EXP(12.72*X))	TABT 570
	DELVIS=6.45E-6*ARHO*EXP(BRHO/T)	TABT 580
	VI=VIS+DELVIS	TABT 590
	XX=RHO/T	TABT 600
	DELXC=3.200E-6*ARHO	TABT 610
	1+XX*(.430011E-5+XX*(.719307E-2+XX*(-.101028+XX*(.493798+XX*(-1.030	TABT 611
	25+XX*(.78894))))))	TABT 612
	IF (T.LT.935.) GO TO 16	TABT 620
	XC=(1.32*W(11)+.12135-.C25/TR)*VIS	TABT 630
	GO TO 17	TABT 640
16	XC=0.604E-5*SQRT(T)/(1.+224.0*(10.**(-12./T))/T)	TABT 650
17	YC=XC+DELXC	TABT 660
	VIG=VI*.0056	TABT 670
	C=XC*.0056	TABT 680
	RETURN	TABT 690
	END	TABT 700

C	SUBROUTINE TABHP(HH,PP,Q,T,V,GA,CP,SV,C,VIG,VIL,VG,VL)	TABHP 10
	NITROGEN	TABHP 20
	DIMENSION A(7),HPP(20),HGG(20),IS(4),IB(4),VN(118)	TABHP 30
	DIMENSION VN1(24)	TABHP 40
	EQUIVALENCE (VN1(1),VN(95))	TABHP 50
	DATA A/.527805,-549.1321,.09133945,-.968802E-3,5.11953E-6,-1.35635	TABHP 60
	1E-8,1.448758E-11/	TABHP 61
	DATA IB/5,4,8,4/	TABHP 70
	DATA IS/1,31,55,95/	TABHP 80
	DATA (VN(I),I=1,94)/	TABHP 90
	1942.64,1912.9,2807.7,3666.0,4505.5,	TABHP 91
	2945.19,1909.5,2802.8,3660.3,4499.4,	TABHP 92
	3947.28,1906.0,2797.8,3654.6,4493.1,	TABHP 93
	4948.80,1902.4,2792.8,3648.8,4486.9,	TABHP 94
	5949.86,1898.9,2787.8,3643.2,4480.7,	TABHP 95
	6950.52,1895.3,2782.9,3637.6,4474.6,	TABHP 96
	7343.22,544.76,745.72,942.64,	TABHP 97
	8370.98,555.92,750.38,945.19,	TABHP 98
	9392.07,565.26,754.24,947.28,	TABHP 99
	9407.85,572.93,757.34,948.80,	TABHP 99
	9419.56,579.09,759.68,949.86,	TABHP 99
	9428.22,583.95,761.38,950.52,	TABHP 99
	9131.72,172.81,208.45,227.00,228.86,253.20,305.42,370.98,	TABHP 99
	9129.36,171.40,210.35,240.93,262.17,290.00,334.33,392.07,	TABHP 99
	9126.91,169.64,210.64,246.71,277.47,310.63,353.81,407.85,	TABHP 99
	9124.37,167.57,210.08,249.44,285.77,323.22,367.14,419.56,	TABHP 99
	9121.77,165.32,208.74,250.52,290.50,331.22,376.36,428.22/	TABHP 99
	DATA VN1/	TABH 100
	1120.00,181.96,262.59,343.22,	TABH 101

2178.00,200.16,272.51,348.77,	TABH 102
3197.00,216.24,281.72,354.32,	TABH 103
4210.00,230.28,290.24,359.88,	TABH 104
5220.00,242.52,298.14,365.43,	TABH 105
6228.26,253.20,305.42,370.98/	TABH 106
KOUNT=0	TABH 110
TCR=110.	TABH 120
QQ=1.	TABH 130
KK=0	TABH 140
ALP=8.	TABH 150
H=HH	TABH 160
P=PP	TABH 170
IF(H.LT.150.) GO TO 6	TABH 180
PP=P/500.	TABH 190
IF(H.LT.300.) GO TC 5	TABH 200
FH=(H-300.)/260.	TABH 210
IG=1	TABH 220
1 IT=PH	TABH 230
IP=FP	TABH 240
PH=AMOD(PH,1.)	TABH 250
FP=AMOD(FP,1.)	TABH 260
IF(H.GE.1340.) GO TO 3	TABH 270
2 IF(P.GT.2500.) GO TC 4	TABH 280
GC TO 13	TABH 290
3 IG=1	TABH 300
IT=3	TABH 310
PH=(H-1340.)/260.+1.	TABH 320
GO TC 2	TABH 330
4 IP=5	TABH 340
FF=(F-2500.)/500.+1	TABH 350
IF(H.LT.150.) IP=4	TABH 360
GO TO 13	TABH 370
5 FH=(H-150.)/50.	TABH 380
IG=2	TABH 390
GO TO 1	TABH 400
6 IF(P.LT.500.) GO TO 8	TABH 410
7 FF=(P-500.)/500.	TABH 420
FH=(H-10.)/20.	TABH 430
IG=3	TABH 440
GO TO 1	TABH 450
8 IF(H.LT.110.) GO TO 10	TABH 460
9 FP=P/100.	TABH 470
FH=(H-110.)/20.	TABH 480
IG=4	TABH 490
GO TO 1	TABH 500
10 IF(P.GE.493.14) GO TO 7	TABH 510
IF(H.LE.3.) GO TO 7	TABH 520
IF(H.GE.105.) GO TC 9	TABH 530
X=33.556-P/14.696	TABH 540
TT=(EXP(4.8293+X*(.619608E-2+X*(-.21951E-2+X*(.124206E-3-X*.23531E-4	TABH 550
1-5)))))*1.8	TABH 551
11 PL=(EXP((A(1)+A(2)/TT+TT*(A(3)+TT*(A(4)+TT*(A(5)+TT*(A(6)+TT*(A(7))))))	TABH 560
1(A(7))))))*2.3025851))*14.696	TABH 561
DPDT=PL*2.3025851*(-A(2)/TT**2+A(3)+TT*(2.*A(4)+TT*(3.*A(5)+TT*(4.*A(6)+TT*(5.*A(7))))))	TABH 570
1*A(6)+TT*(5.*A(7))))))	TABH 571
IF(ABS(P-PL).LT.0.001) GO TO 12	TABH 580
TT=TT+(P-PL)/DPDT	TABH 590
KOUNT=KOUNT+1	TABH 600
IF(KOUNT.LT.20) GC TO 11	TABH 610
12 CALL TABTP(TT-.01,P,HP,VL,GAL,CPL,SVL,CI,VIL,ICE)	TABH 620
KOUNT=0	TABH 630
IF(H.LT.HP) GO TO 14	TABH 640
CALL TABTP(TT+.01,P,HG,VG,GAA,CPV,SVV,CC,VIGG,ICE)	TABH 650
IF(H.GT.HG) GO TO 22	TABH 660
QQ=(H-HP)/(HG-HP)	TABH 670
VV=QQ*VG+(1.-QQ)*VI	TABH 680
GO TO 25	TABH 690

13	PH1=1.-PH	TABH 700
	PP1=1.-PP	TABH 710
	P11=PH1*PP1	TABH 720
	P12=PH*PP1	TABH 730
	P21=FP*PH1	TABH 740
	P22=FP*PH	TABH 750
	L=IS (IG) +IT+IP*IB (IG)	TABH 760
	I=L+ID (IG)	TABH 770
	TT=P11*VN (L) +P12*VN (L+1) +P22*VN (I+1) +P21*VN (I)	TABH 780
	GO TO 23	TABH 790
14	TT=TT-.01	TABH 800
	QQ=0.	TABH 810
	TCR=227.268	TABH 820
	GO TO 23	TABH 830
15	IF (DH) 16,25,19	TABH 840
16	IF (KK-1) 17,18,21	TABH 850
17	KK=1	TABH 860

18	CRL=ALP	TABH 870
	GO TO 24	TABH 880
19	IF (KK-1) 20,21,18	TABH 890
20	KK=2	TABH 900
	GO TO 18	TABH 910
21	ALP=ALP/2.	TABH 920
	GO TO (2U,17),KK	TABH 930
22	TT=TT+.01	TABH 940
23	CALL TABTP (TT,P,H1,VV,GAA,CPP,SVV,CC,VIGG,ICE)	TABH 950
	DH=H-H1	TABH 960
	IF (ABS (DH) .LT.0.01) GO TO 25	TABH 970
	CRL=.25*ABS (TT-TCR)	TABH 980
	IF (KOUNT.GT.9) GO TO 15	TABH 990
24	TT=TT+SIGN (AMIN1 (ABS (DH/ CPP),CRL),DH)	TAB 1000
	IF (TT.LT.120.) TT=120.	TAB 1010
	KOUNT=KOUNT+1	TAB 1020
	IF (KOUNT.LT.40) GO TO 23	TAB 1030
25	Q=QQ	TAB 1040
26	T=TT	TAB 1050
	V=VV	TAB 1060
	GA=GAA	TAB 1070
	CP=CPP	TAB 1080
	SV=SVV	TAB 1090
	C=CC	TAB 1100
	VIG=VIGG	TAB 1110
	RETURN	TAB 1120
	END	TAB 1130

SUBROUTINE XTERM (RHH,RHL,X1,X2)	XTERM 10
COMMON /XDRTN2/XN,T,TS,TSS,R,AK,XJ	XTERM 20
DIMENSION XK (5),XN (16),XJ (7)	XTERM 30
X3=RHH*RHH	XTERM 40
X4=RHL*RHL	XTERM 50
X5=X3*XN (16)	XTERM 60
X6=X4*XN (16)	XTERM 70
X7=RHH-RHL	XTERM 80
X8=EXP (X5)	XTERM 90
X9=EXP (X6)	XTERM 100
X10=(X8-X9)/(2.*XN (16))	XTERM 110
X11=(X8*(X5-1.)-X9*(X6-1.))/(2.*XN (16)**2)	XTERM 120
X1=((20.*XN (5)/TS+6.*XN (4))/T+2.*XN (3))/TS)*17 *	XTERM 130
1*((20.*XN (11)/T+12.*XN (10))/T+6.*XN (9))/TSS)*11C *	XTERM 131

[illegible]

```

SUBROUTINE NIT900 (T, PP, W)
  RANGE TEMP 900 TO 4500 DEG RANKINE - PRESSURE C-2500 PSIA  NIT90 20
  DIMENSION W(6), VN(155)
  DIMENSION VN1(30), VN2(30), VN3(30), VN4(30), VN5(5)
  EQUIVALENCE (VN1(1), VN(31)), (VN2(1), VN(61)), (VN3(1), VN(91)), (VN4(1), VN(121)), (VN5(1), VN(151))
  ENTHALPY BTU/LE
  DATA (VN(I), I=1, 30)/
  1288.69, 527.39, 787.42, 1059.56, 1338.29,
  2287.93, 528.30, 788.88, 1061.30, 1340.19,
  3287.29, 529.25, 790.37, 1063.08, 1342.14,
  4286.80, 530.22, 791.86, 1064.84, 1344.07,
  5286.44, 531.19, 793.34, 1066.58, 1345.99,
  6286.19, 532.18, 794.80, 1068.31, 1347.89/
  COMPRESSIBILITY FACTOR Z=P*V/(R*T)
  DATA VN1/
  11., 1., 1., 1., 1.,
  21.01497, 1.01404, 1.01086, 1.00871, 1.00724,
  31.03099, 1.02796, 1.02157, 1.01732, 1.01441,
  41.04790, 1.04174, 1.03216, 1.02583, 1.02151,
  51.06555, 1.05540, 1.04263, 1.03425, 1.02853,
  61.08379, 1.06892, 1.05297, 1.04257, 1.03549/
  SPECIFIC HEAT RATIO GA=CP/CV
  DATA VN2/
  11.392, 1.341, 1.313, 1.301, 1.294,
  21.412, 1.345, 1.315, 1.302, 1.294,
  31.430, 1.350, 1.317, 1.303, 1.295,
  41.447, 1.354, 1.319, 1.304, 1.296,
  51.461, 1.358, 1.321, 1.305, 1.296,
  61.474, 1.361, 1.322, 1.306, 1.297/
  SPECIFIC HEAT -CP-
  DATA VN3/
  1.25230, .27878, .29708, .30670, .31222,
  2.25609, .27970, .29749, .30693, .31237,
  3.25964, .28060, .29790, .30717, .31253,
  4.26282, .28144, .29830, .30741, .31268,
  5.26567, .28224, .29869, .30764, .31283,
  6.26821, .28300, .29906, .30787, .31298/
  SONIC VELOCITY
  DATA VN4/
  117893., 24834., 30097., 34594., 38573.,
  218153., 25243., 30283., 34758., 38712.,
  318413., 25264., 30465., 34919., 38864.,
  418673., 25470., 30646., 35078., 39015.,
  518921., 25499., 30825., 35235., 39148.,
  619167., 25867., 30989., 35389., 39296./
  SPECIFIC HEAT -CVC-
  DATA VN5/, 18125., 20788., 22626., 23574., 24128/
  T=TT
  P=PP
  PT=(T-900.)/900.
  PP= P/500.
  IT=PT
  IP=PP
  PT=AMOD(PT, 1.)
  PP=AMOD(PP, 1.)

```



```

IF (T.LE.4500.) GO TC 1
IT=3
TR=(T-4500.)/900.
FT=TR+1.
1 IF (P.LE.2500.) GO TC 2
IP=4
PR=(P-2500.)/500.
PP=PR+1.
2 PT1=1.-PT
FP1=1.-PP
P11=PT1*PP1
F12=PT*PP1
P21=PP*PT1
F22=PP*PT1
L=1+IT+IP*5
DO 3 K=1,5
J=L+ (K-1)*30
I=J+5
3 W(K)=P11*VN(J)+F12*VN(J+1)+F22*VN(I+1)+F21*VN(I)
W(2)=661.95*W(2)*I/F
L=151+IT
W(6)=PT1*VN(L)+FT*VN(L+1)
RETURN
END

```

NIT9 260
NIT9 270
NIT9 280
NIT9 290
NIT9 300
NIT9 310
NIT9 320
NIT9 330
NIT9 340
NIT9 350
NIT9 360
NIT9 370
NIT9 380
NIT9 390
NIT9 400
NIT9 410
NIT9 420
NIT9 430
NIT9 440
NIT9 450
NIT9 460
NIT9 470
NIT9 480
NIT9 490

```

SUBROUTINE NITRO(TEMP,PRES,V,HH,VS,GA,CF)
DIMENSION TID(17),HID(17),CVID(17)
DIMENSION XK(5),XN(16),XJ(7)
COMMON /XDRIN2/XN,T,TS,ISS,R,XK,XJ
DATA TID/66.666,72.222,77.777,83.333,88.888,94.444,100.,105.555,
111.111,116.666,119.444,122.222,124.444,125.555,125.833,126.111,
2126.26/
DATA HID/202.86,525.25,847.11,1169.4,1454.1,1827.5,2177.2,2551.4,
12959.5,3396.5,3648.0,3942.8,4241.3,4437.5,4497.1,4562.5,4601.0/
DATA CVID/29.7,27.8,25.7,26.0,25.4,24.2,24.1,23.9,
124.727,26.118,27.208,28.649,30.180,31.174,31.474,31.804,32.000/
T=TEMP/1.8
P=PRES/14.696
RT=P*T
TS=T*T
TSS=TS*T
J=0
ITYPE=1
CPO=2.910996E+1 + T*(-8.0820995E-4 + T*(8.6142037E-6 + T*
1*(-3.6893728E-8 + 1* 5.6750880E-11)))
HC=4226.3003+T*(29.109996+T*(-4.0410497E-4+T*(2.8714012E-6+T*
1*(-.9223307E-8+T*(1.1350176E-11))))
CVO=CPO-R/.00986896
IF (T.GE.126.26) GO TC 1
X= (XJ(1)+XJ(2))/T+T*(XJ(3)+T*(XJ(4)+T*(XJ(5)+T*(XJ(6)+T*XJ(7))))
1))
PP=10.**X
IF (P.LT.PP) GO TO 1
PSAVE=P
P=PP
ITYPE=2
X=(1.-T/126.26)**.33333333
RHO=XK(1)+X*(XK(2)+X*(XK(3)+X*(XK(4)+X*(XK(5))))
GO TC 2
1 RHO=P/RT
2 A=R*XN(1)*T+XN(2)+(((XN(5)/TS+XN(4))/T+XN(3))/T)
B=R*XN(6)*T+XN(7)
F=XN(8)*T

```

NITRO 10
NITRO 20
NITRO 30
NITRO 40
NITRO 50
NITRO 51
NITRO 52
NITRO 60
NITRO 61
NITRO 70
NITRO 71
NITRO 80
NITRO 90
NITR 100
NITR 110
NITR 120
NITR 130
NITR 140
NITR 150
NITR 151
NITR 160
NITR 161
NITR 170
NITR 180
NITR 190
NITR 191
NITR 200
NITR 210
NITR 220
NITR 230
NITR 240
NITR 250
NITR 260
NITR 270
NITR 280
NITR 290
NITR 300
NITR 310

	C=((XN(11)/T+XN(10))/T+XN(9))/TS)	NITR 320
	C=((XN(14)/T+XN(13))/T+XN(12))/TS)	NITR 330
	DA=R*XN(1)-(((4.*XN(5)/TS+2.*XN(4))/T+XN(3))/TS)	NITR 340
	DB=R*XN(6)	NITR 350
	DC=-(((4.*XN(11)/T+3.*XN(10))/T+2.*XN(9))/TSS)	NITR 360
	DD=-(((4.*XN(14)/T+3.*XN(13))/T+2.*XN(12))/TSS)	NITR 370
3	RHOS=RHO*RHO	NITB 380
	EX=FXP(XN(16)*RHCS)	NITR 390
	EC=EX*C	NITR 400
	ED=EX*D	NITR 410
	PC=RHO*(RT+RHO*(A+RHO*(E+EC+RHO*(E+RHC*(ED+RHC*XN(15))))))	NITR 420
	DPDR=RT+RHO*(2.*A+RHO*(3.*B+3.*EC+RHO*(E+4.*RHO*(5.*ED+2.*XN(16))))))	NITR 430
	J=J+1	NITR 440
	IF(J.GT.30) GO TO 6	NITB 450
	IF(ABS((P-PC)/P).LT..0001) GO TO 7	NITB 460
	DP=P-PC	NITB 470
	IF(T.GE.126.26) GO TO 4	NITR 480
	CRLIMT=0.25*ABS(RHC-11.230207)+1.	NITB 490
	GO TO 5	NITR 500
4	CRLIMT=.25*RHO	NITR 510
5	CONTINUE	NITR 520
	RHO=RHO*SIGN(AMIN1(ABS(DP/DPDR),.25*RHC,CRLIMT),DP)	NITR 530
	GO TO 3	NITR 540
6	WRITE(6,1001)P,PC	NITR 550
1001	FORMAT(17H NCN CONVERGENCE,2E14.4)	NITR 560
7	GO TO(12,8,9),ITYPE	NITR 570
8	SRHO=RHO	NITR 580
	ITYPE=3	NITR 590
	P=PSAVE	NITR 600
	J=0	NITR 610
	GO TO 3	NITR 620
9	DO 10 J=2,17	NITR 630
	IF(T.LT.TID(J)) GO TO 11	NITR 640
10	CONTINUE	NITR 650
11	X=(T-TID(J-1))/(TID(J)-TID(J-1))	NITR 660
	HO=HID(J-1)+X*(HID(J)-HID(J-1))	NITR 670
	CVRL=CVID(J-1)+X*(CVID(J)-CVID(J-1))	NITR 680
	CALL XTERM(RHC,SRHC,TERM1,TERM2)	NITR 690
	CVR=CVR-TERM1/.00986896	NITR 700
	H=HO+(P/RHO-PP/SRHO+TERM2)/.00986896	NITR 710
	GO TO 13	NITD 720
12	CALL XTERM(RHO,0.,TERM1,TERM2)	NITR 730
	CVR=CVR-TERM1/.00986896	NITR 740
	H=HO+(TERM2+P/RHO-RT)/.00986896	NITR 750
13	DPDT=RHO*(R+RHO*(CA+RHO*(DB+DC*EX+RHO*(XN(8)+RHC*(DD*EX))))	NITR 760
	CPR=CVR+T*(DPDT/RHO)**2/DPDR/.00986896	NITR 770
	GA=CPR/CVR	NITR 780
	VS=SQRT(5.6058E+6*GA+DPDR)	NITR 790
	V=988.024/RHO	NITB 800
	HH=.01534880*H	NITR 810
	CP=0.00852711*CPR	NITB 820
	RETURN	NITR 830
	END	NITR 840

BLOCK DATA	10
DIMENSION XK(5),XN(16),XJ(7)	20
COMMON /XDRTN2/XN,I,TS,TSS,R,XK,XJ	30
DATA XK/11.230207,21.082073,-9.8177403,27.790397,-11.764704/	40
DATA R,XN/.0820574,.3371608442E-1,-.5771942866,-.1142108127E+3,	50
1.8522634899E+3,.34401762E+7,.1650365874E-2,-.157890591E-1,	51
2.4168356912E-5,.3211549057E+3,.1080120452E+6,-.1066657899E+8,	52
3-.3304489192E+1,.1223693626E+4,-.5693539048E+5,.1675167178E-5,	53
4-.0056/	54
DATA XJ/-.527805,-305.07339,.16441101,-3.1389205E-3,2.9857103E-5,	60
1-1.4238458E-7,2.7375282E-10/	61
END	70

```

      SUBROUTINE BIGAR(FFA,FEFA,PFH,REFZ,FEEST,RE,FFS,FEESTH,REZ,K,FPAA,
      1FEFAA,PFHA,REFZA,FEESTA,REA,FFSA,FSHA,FEZA)
C   FOR STORING PP RE ,ST FUNCTION FOR MULTI-RUN PLOTS
      DIMENSION FFA(50),FEFA(50),PFH(50),REFZ(50),FEEST(50),RE(50),
      1      FPAA(50),FEFAA(50),PFHA(50),REFZA(50),FEESTA(50),REA(50),
      2FEESTH(50),REZ(50),FEZA(50),FFSA(50),FSHA(50)
      FPAA(K) = FFA(5)
      FEFAA(K) = FEFA(5)
      PFHA(K) = PFH(5)
      REFZA(K) = REFZ(5)
      FEESTA(K) = FEEST(5)
      REA(K) = RE(5)
      FFSA(K) = .118 * REFZ(5)**(-.155)
      FSHA(K) = FEESTH(5)
      FEZA(K) = REZ(5)
      RETURN
END BIGAR

```

```

      SUBROUTINE PLFFA
C   FOR PLOTTING ANNULUS PP VS RP
      DIMENSION XD(2),TD(2),BUFFER(6000)
      XD(1) = 10000.
      XD(2) = 1000000.
      TD(1) = .012
      TD(2) = .05
      CALL SETPLT(XD,TD,-2,'LCG','MECH',0.,0.,BUFFER,6000)
      CALL LABEL(2,.3,'ANNULUS FRICTION FACTORS$',-1)
      CALL LABEL(1,.125,'REYNOLDS MODULUS BASED ON FILM DENSITY AND
      1 VISCOSITY,BULK VELOCITY$',-1)
      CALL LABEL(-1,.125,'FRICTION FACTOR (ELASIOS) $',-1)
      RETURN
END PLFFA

```

```

      SUBROUTINE PLFFH
C   FOR PLOTTING ROD PP
      DIMENSION XD(2),TD(2),BUFFER(6000)
      XD(1) = 10000.
      XD(2) = 1000000.
      TD(1) = .012
      TD(2) = .08
      CALL SETPLT(XD,TD,-2,'LCG','MECH',0.,0.,BUFFER,6000)
      CALL LABEL(2,.3,'ROD FRICTION FACTORS$',-1)
      CALL LABEL(1,.125,'REYNOLDS MODULUS BASED ON FILM DENSITY AND
      1 VISCOSITY,BULK VELOCITY$',-1)
      CALL LABEL(-1,.125,'FRICTION FACTOR (ELASICS) $',-1)
      RETURN
END PLFFH

```

```

      SUBROUTINE PLSTA
C   FOR PLOTTING ANNULUS STANTON FUNCTION
      DIMENSION XD(2),TD(2),BUFFER(6000)
      XD(1) = 10000.
      XD(2) = 1000000.
      TD(1) = .001
      TD(2) = .005
      CALL SETPLT(XD,TD,-2,'LCG','MECH',0.,0.,BUFFER,6000)
      CALL LABEL(2,.3,'FUNCTION F(ST) $',-1)
      CALL LABEL(1,.125,'BULK REYNOLDS MODULUS$',-1)
      CALL LABEL(-1,.125,'F(ST) $',-1)
      RETURN
END PLSTA

```

```

      SUBROUTINE PLSTAH
C   FOR PLOTTING ROD STANTON FUNCTION
      DIMENSION XD(2),TC(2),BUFFER(6000)
      XC(1) = 10000.
      XD(2) = 1000000.
      TD(1) = .002
      TD(2) = .008
      CALL SETPLT(XD,TD,-2,'LCG','MECH',0.,0.,BUFFER,6000)
      CALL LABEL(2,.3,'FUNCTION P(ST)$',-1)
      CALL LABEL(1,.125,'EULK REYNOLDS MODULUS$',-1)
      CALL LABEL(-1,.125,'P(ST)$',-1)
      RETURN
END PLSTAH

```

THIS PAGE
WAS INTENTIONALLY
LEFT BLANK

INTERNAL DISTRIBUTION

- | | |
|----------------------------|--|
| 1. T. D. Anderson | 46. R. N. Lyon |
| 2. H. F. Bauman | 47. R. E. MacPherson |
| 3. S. E. Beall | 48. W. J. McCarthy |
| 4. R. F. Bennett | 49. H. A. McLain |
| 5. R. H. Chapman | 50. S. L. Milora |
| 6. D. L. Clark | 51. R. C. Robertson |
| 7. S. K. Combs | 52. M. W. Rosenthal |
| 8. W. B. Cottrell | 53. J. P. Sanders |
| 9. G. G. Fee | 54. W. K. Sartory |
| 10. M. H. Fontana | 55. J. D. Sheppard |
| 11. A. P. Fraas | 56. M. J. Skinner |
| 12. D. D. Gray | 57. I. Spiewak |
| 13. M. J. Goglia | 58. J. J. Taylor |
| 14-18. H. W. Hoffman | 59. D. G. Thomas |
| 19. R. S. Holcomb | 60. D. B. Trauger |
| 20. L. Jung | 61. J. P. White |
| 21. P. R. Kasten | 62. G. D. Whitman |
| 22. G. J. Kidd, Jr. (K-25) | 63. W. J. Wilcox |
| 23-42. O. H. Klepper | 64-65. Central Research Library |
| 43. T. S. Kress | 66. Document Reference Section |
| 44. M. E. LaVerne | 67-69. Laboratory Records Department |
| 45. C. G. Lawson | 70. Laboratory Records Department (RC) |

EXTERNAL DISTRIBUTION

- 71. Research and Technical Support Division, ERDA, ORO
- 72. Director, Reactor Division, ERDA, ORO
- 73-74. Director, Division of Reactor Research and Development, ERDA,
Washington, DC 20545
- 75-218. For distribution as shown in TID-4500 under category UC-77,
Gas Cooled Reactor Technology